CHALMERS

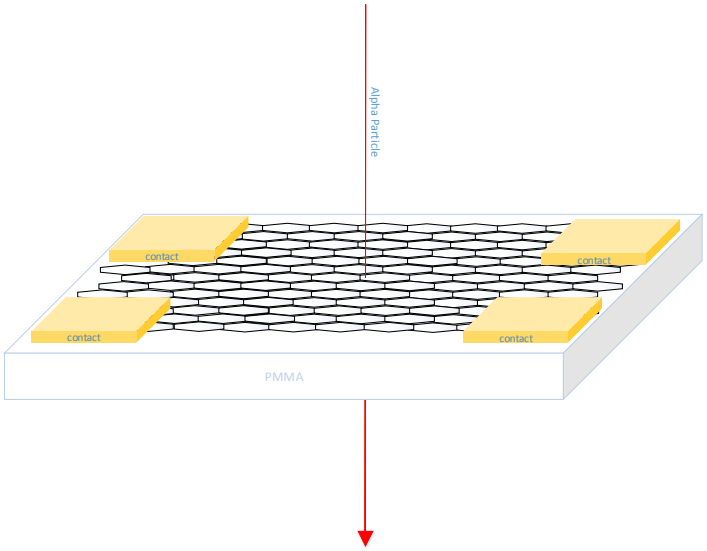

Using Graphene As Ion Detector

Master's thesis in Erasmus Mundus of Nanoscience and Nanotechnology

M. JAUHAR KHOLILI

Department of Fundamental Physics
CHALMERS UNIVERSITY OF TECHNOLOGY
Gothenburg, Sweden 2015

Education and Culture DG
ERASMUS MUNDUS

KATHOLIEKE UNIVERSITEIT LEUVEN

Master's thesis 2015

Using Graphene as Ion Detector

M. JAUHAR KHOLILI

CHALMERS
UNIVERSITY OF TECHNOLOGY

Department of Fundamental Physics
Subatomic Physics group
Chalmers University of Technology
Gothenburg, Sweden 2015

Using Graphene as Ion Detector
M. JAUHAR KHOLILI

Supervisor: Thomas Nilsson, Department of Fundamental Physics, Chalmers
Examiner: Andreas Heinz, Department of Fundamental Physics, Chalmers
Co-promotor: Jin Won Seo, Department of Material Engineering, KU Leuven

Master's Thesis 2015
Department of Fundamental Physics
Subatomic Physics group
Chalmers University of Technology
SE-412 96 Gothenburg
Telephone +46 31 772 1000

Cover: Visualization of penetration of an α-particle through the graphene and the PMMA film.

Typeset in LaTeX
Printed by Chalmers Reproservice
Gothenburg, Sweden 2015

Using Graphene as Ion Detector

M. Jauhar Kholili
Department of Fundamental Physics
Subatomic Physics Group
Chalmers University of Technology

Abstract

Graphene is a new type material that attracts attentions of worldwide research communities since Andre Geim and Konstantin Novoselov fabricated freestanding graphene in 2005 successfully. Its exceptional mechanical, chemical, structural and electronic properties make graphene projected as a candidate for substituting present semiconductor technology for various electronic applications in the future. Although various graphene detector applications already studied by many groups, graphene for particle detector application is one topic, that is missed from attention.

A single layer graphene with dimension 1 cm x 1cm on the top of thin PMMA and ZEP film is utilized in this experiment. By exposing the graphene with alpha particle perpendicularly in a vacuum condition, the measurement about graphene electronic responses are characterized by two-point resistance measurements. Besides, the number of α-particles and their energy loss are measured by nuclear data acquisition system.

The results show that a single layer graphene is highly permeable and almost transparent toward alpha particles penetration by absorbing insignificant part of their energy. However, a single layer graphene is also very sensitive to external parameter such as ambient gases and pressure change.

Keywords: Graphene, Detector, α-particles

Contents

Acknowledgements

The thesis could not have been finished without help of so many people which all deserve to be thanked. First and foremost, I would like to thank to my Advisor, Andreas Heinz who patiently help throughout the project, provide insightful thoughts, comment on the work and later proof reading my thesis.

Secondly I want to thank to my supervisor Thomas Nilsson who gave me the opportunity to work in this master thesis project. I am also thankful for the help of my co-promotor Jin Won Seo who provided her time to review my thesis. I am also grateful for the help of our collaborators, Avgust Yurgens and Grigory Soblin who provided us the samples and whom I later had alot of dicussion regarding of the experiments. I am very happy to have discussion with Håkan Johansson and Simon Lindberg who has helped me with some technical issues and answered my questions. I am also thankful to the whole research group of Fundamental Physics at Chalmers, the input from the group meeting always give new sights for my experiment.

Lastly but not least, I would like to thank to my family especially my parents, Muntamah and Ali Ma′sum, for always supporting me spiritually throughout my life and also to my friend from Laskar Göteborg for sharing laugh together every week end.

M. Jauhar Kholili, Gothenburg 2015/08/20

1

Introduction

Graphene is a new type of material that attracts the attention of the worldwide research communities since Andre Geim and Konstantin Novoselov fabricated free-standing graphene fot the first time in 2005 successfully. Its exceptional mechanical, chemical, structural and electronic properties make graphene a candidate for substituting present semiconductor technology in various electronic applications in the future. One of the many areas which graphene has been developed massively after its invention is for detector applications. Graphene has been used as sensitive photodetector [1, 2, 3], gas detector [4, 5, 6, 7], chemical detector [8, 9, 10], biomolecular detector [11, 12] among others. Although various detector applications are already studied by many groups, the use of graphene for particle detector applications is a topic that has not been studied so far.

Some graphene properties that might make it an ideal material for a particle detector are its robustness (Young's modulus is 1 TPa and its intrinsic strength 130 Gpa) [13], its high electron current density [14], and its high electron mobility at room temperature (2.5 x $10^5 cm^2$ V^{-1} s^{-1})[15]. Transistor applications shows that graphene can work with a cut-off frequency above 1 GHz [16, 17] proving that graphene has a very fast response, indicating high rate capability. Furthermore, graphene is also relatively durable from defects under irradiation of particle [18]. Therefore, the graphene layer is expected to overcome these classic problems with high endurance.

The detection of swift heavy ions with low kinetic energies with a range from some hundreds of keV to a few MeV is a tricky problem. Conventional detectors decrease the energy of low-energy ions significantly, and deviate the ion trajectory and due to angular straggling. Eventually, precise information about the type of the ion is hard to obtain. The purpose of this thesis is for investigate the possibility of measuring the Time of Flight (TOF) of an ion using a graphene detector. Single-layer graphene with the dimension 1 cm x 1cm on top of a thin PMMA film is utilized in this experiment. By exposing the graphene to alpha particles crossing it perpendicular in a vacuum chamber, signals from current generation is expected to be produced in graphene layer. Furthermore, to characterize the change of the properties of graphene during the experiment, two-point resistance measurements are carried out.

2

Theory

2.1 Graphene

Graphene is the first two-dimensional (2D) material that has been produced in freestanding condition successfully. A single layer of graphene with a thickness 0.335 nm [19] has a mechanical structure stronger than steel with same weight [13, 20] and it has better electronic conductivity than copper and silver [21]. The superior electrical and mechanical properties of graphene originate from the unique hexagonal honeycomb structure of the carbon atom. The sp_2 hybridization of the carbon atom results in hybridized s, p_x and p_y atomic orbitals. These hybridized atomic orbitals are strongly bound to the three nearest carbon atom with σ-bonds. Non-hybridized p_z atomic orbitals result in two p_z orbital bands. The first p_z orbital band is filled with one electron and bound with an electron from a nearest atom carbon. This configuration forms an additional bond called the π bond. This π bond configuration allows for graphene to have three double bonds in its hexagonal structure. Furthermore, this filled p_z orbital also results in the valence band of graphene. The second unhybridized p_z orbital band is empty. The empty p_z orbital produces the conduction band of graphene.

The energy dispersion relation of graphene forms double cone-like energy band (Dirac-cone) with a zero band gap shown in fig. 2.1.a. This fact gives graphene peculiar electronic characteristics. Unlike semiconductor and metal, graphene does not have a bandgap nor a half-filled conduction band. Therefore graphene is classified as semimetal. The cone-like energy dispersion relation results in the fact that all of the electrons in graphene have a uniform velocity ($v_g = dE/dk$) as if the electrons have no inertia. Therefore, a very high conductivity can be reached in graphene. For the pristine single layer graphene without any external electric and magnetic field, the Fermi energy is at the K point, the point where the two oppositely directed cones-shaped valence and conduction bands meet.

The graphene response to an electronic input signal is inversely proportional to a graphene dimension [16] for graphene transistor that has a size less than 1 μm. The input signal for the graphene transistor is an electric field which penetrates the graphene layer perpendicular. A parameter to measure the maximum response of a device is called cut-off frequency. The cut-off frequency is the highest frequency of an input signal before the output becomes indistinguishable for both the on-state

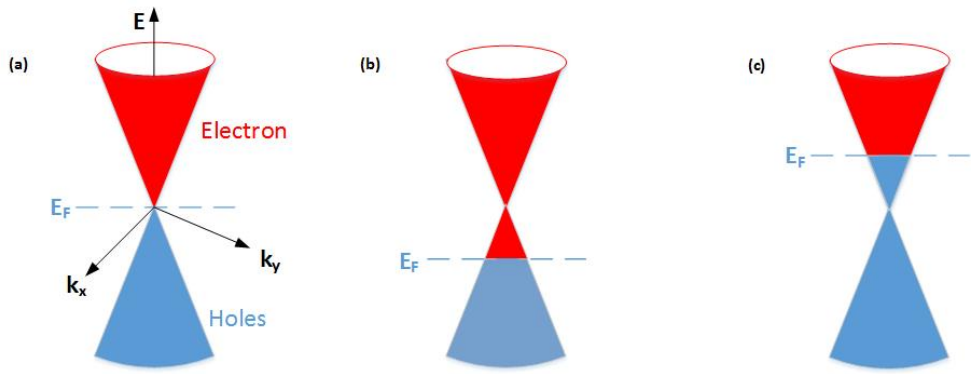

Figure 2.1: (a) Band structure of graphene. (b) n-type of graphene. (c) p-type of graphenen.

and the off-state. The on-state is the condition when graphene is penetrated by the electric field and off-state when there is no electric field influencing graphene. The larger the dimension, the smaller cut-off frequency of the graphene device. For the case of graphene transistor that has a gate length from 40 nm to 550 nm, the relation between the treshhold frequency f_t and graphene gate length L_g is always consistent with equation $f_t L_g = 13$ GHz μm [16]. If the trend is still working for much larger graphene size, a graphene with dimension 1 cm should have a cut-off frequency about 1 MHz. It is still suitable for particle detector setup that is designed to detect particle with a rate about 10000 particle/second.

2.1.1 Modification of the Electronic Properties of Graphene

Understanding the electronic properties of a material is the first fundamental step for adopting a material for most applications.There are three common mechanisms that affect the electronic properties of graphene. Those are: applying a bias voltage to build up an electric field, doping and controlling the dimension. In the neutral condition, graphene has a low concentration of both types of carriers. The electrons and holes are symmetric in number, and their density is low. Exposing graphene to an electric field and doping breaks the symmetry of both carriers. It means one carrier become majority carrier and the other become minority carrier. Correspondingly, similar to a semiconductor, graphene can be n-type or p-type graphene. Shrinking the size of graphene can increase the band gap in graphene, which is one important key factor to use graphene for device that are traditionally bases on semiconductor technology.

Graphene is an ambipolar material that can have either majority carrier by applying an electric field of the appropriate polarity and magnitude. An electric field or doping of a graphene layer results in shifting of the Fermi energy and defining the majority carrier (electrons or holes). The shifting of Fermi level upward (downward) means that the holes (electron) are the majority carrier of the graphene (fig. 2.1.b and fig. 2.1.c). A further shift of Fermi energy from Dirac point increase the

number of the carriers. A perpendicular electric field can result in n-type or p-type of graphene depending on its polarity. For pristine graphene, the lowest conductivity would be found if no electric field is applied because of the graphene layer is in its neutral condition and does not have abundant carriers. If the electric field penetrates graphene layer in perpendicular direction, it will create more holes or electrons to in graphene layer. The stronger electric field produces a higher the conductivity because more carriers are created.

Another way that change the electronic properties of graphene is by doping it. There are two type of doping, the chemical doping and self-doping. Chemical doping is a method to add foreign molecules to graphene chemically. On the other hand, self-doping shifts the Fermi energy of graphene because the lattice defects and lattice boudaries.

There are two categories of chemical doping, surface transfer doping, and substitutional doping. Both types result in extrinsic n-type (p-type) graphene with electrons (holes) as majority carrier. For surface transfer doping, the molecule is deposited on top of a graphene layer without disturbing the 2D structure of graphene. Surface transfer doping works if the molecule and the graphene interchange electrons at their interface. The electron transfer of doping and graphene depends on the Density of States (DOS) in graphene. If the Highest Occupied Molecular Orbital (HOMO) of the doping molecule is higher than the Fermi energy of the graphene, the electrons are transferred from the doping molecule to graphene resulting in n-type graphene. On the other hand, if the Lowest Unoccupied Molecular Orbital (LUMO) of the doping molecule is lower than the Fermi level of graphene, the electrons of graphene are transferred to the doping molecule resulting in p-type graphene [22]. The standard methods to realize this kind of doping are by spin coating and deposition processes.

The contact in a graphene device is normally made from metal that has a high conductivity. This metal also acts as doping that works based on electrons exchange mechanism. The doping mechanism resulted from metal contact is classified as surface transfer doping. The shifting of Fermi energy of graphene depends on the difference between the work function of the graphene and the metal. Pristine graphene has a work function of 4.5 eV [23], but the transition point is not exactly at the magnitude of graphene work function. At equilibrium distance between the atoms of metal and graphene, the transition point whether a metal dopes holes or electron to a graphene layer is +0.9 eV higher than the work function of graphene [22]. The metals that have a work function higher (lower) than the transition point dopes graphene with holes (electrons). Thus, metals contact that results n-type of graphene are Aluminum (Al), Silver (Ag), and Copper (Cu). The work functions are 4.08 eV for Aluminum, 4.26-4.73 eV for silver and 4.7 eV for copper. On the other hand, metals that result in p-type of graphene are Gold (Au) and Platinum (Pt) that have work function of 5.1 eV, and 6.35 eV respectively [24, 25]. However, Al, Ag, and Cu are a type of metal that have a weak interaction with graphene. Therefore, they can dope graphene with the opposite carriers in larger distance between metal

atoms and graphene because the transition point is lower.

Supporting substrate of graphene also has a role as doping. For graphene with poly(methyl methacrylate) (PMMA) as supporting substrate, the PMMA film can behave as p-type doping for graphene [26]. PMMA tends to trap positive charges resulting in a net density of positive charges in the graphene layer. On the other hand, during ion radiation, the electronic properties of graphene can be changed because part of the energy of ions is stored along the ion track in the substrate. Typically, a substrate is made from semiconductor or insulator material that cannot dissipate the energy rapidly. Therefore, the energy concentrated in a small volume becomes sufficient to eject the substrate particles (Fig. 2.2). Those ejected substrate atoms dope the graphene layer and finally change the electrical properties of graphene [27].

Figure 2.2: The local heating created while ion is passing through the substrate is concentrated in narrow area and ejects some of substrate atoms to dope graphene layer.

Substitutional doping methods disrupt the hexagonal structure of graphene and replace some carbon atoms with the doping atoms, forming a covalent bond. Each of carbon atom in a graphene layer has four valence electrons. If the molecules have more valence electron than carbon e.g. Boron, this doping results in n-type graphene. The remaining electron of the doping material is not bonding with another electron from surrounding carbon atoms, so it is relatively free to escape when there is external disturbance such as an electric field. However, if doping molecules have fewer valence electrons than carbon, only three valence electrons from this doping atom bond with surrounding carbon atoms. This leaves an electron from an unbound carbon atom resulting in a hole. The unbound electron of carbon atom in the vicinity could easily move to fill the space creating quasi-movement of the holes.

Graphene is one of the most sensitive materials with respect to the influence of the surrounding environment. Any substances including nitrogen [28, 22], oxygen [29, 22] and water vapor [22] that are abundant in the atmosphere can be bound chemically or physically to graphene. The physical bonding of molecules to graphene surface occurs by a rapid physisorption processes involving the weak Van der Waals

force (about 10–100 meV). On the other hand, chemical bonding of molecule to graphene surface occures by a slower chemisorption processes involving the stronger covalent bonds (about 1-10 eV). In the sense of reversibility, there are two types of chemical doping for graphene, reversible doping, and irreversible doping. The reversible doping is a type of doping that can be removed from graphene using e.g. heating and pumping. For example, annealed graphene is reversibly doped by dry oxygen in a short time exposure. On the other hand, oxygen that dopes annealed graphene in wet condition for relatively longer time exposure is an example for the irreversible doping that has stronger covalent bounds [23].

These bound gasses change the electrical properties of graphene because these foreign materials are behaving as doping for graphene. The most likely unintended doping substance from the atmosphere are oxygen, water vapor, and nitrogen. Oxygen and water vapor result in p-type doping of graphene while nitrogen produces n-type doping [22]. Compared to other gasses in the atmosphere, oxygen is the primary factor that graphene in the ambient atmosphere is doped [23]. Exposure to oxygen results in O_2 bind covalently with sp_2 hybridized carbon atoms forming sp_3 carbon hybridization [30] in graphene's honeycomb ring structure. Some of the electrons in the graphene structure are transfered to oxygen that resulting in p-type doping.

Self-doping effects are present because of lattice defects in graphene such as grains boundaries or cracks. During the process of fabrication, transfer, handling and measurement, the mechanical properties of graphene, that tends to be brittle, makes the creation, and propagation of cracks relatively easy. The grain boundaries and cracks produce electrostatic potential along their length and shift the position of the Fermi energy of the graphene layer. For a large area of graphene, the self-doping effect is negligible because the effect is inversely proportional to the width of the graphene layer. It is only very significant in a nanoribbon with a width of the order of nanometers.

By controlling the size graphene, a bandgap can be produced in its energy band. This phenomenon is commonly observed in a graphene nanoribbons. The value of the bandgap in graphene nanoribbon is inversely proportional to its width. The width of graphene nanoribbon that can produce a significant band gap should be below 0.1 μm [31]. Therefore, this method is not suitable for applications that use large areas of graphene. However, opening a band gap of large area bilayer graphene could be achieved by applying perpendicular causing a band gap of about 0.2 eV in bilayer graphene [32]. However, this band gap value is still much smaller than the bandgap of silicon that is about 1.1 eV.

2.1.2 Characterization of Graphene

Graphene is a material that is very sensitive to internal and external perturbations. The build-up of defects and impurities during the transfer and storing before

an experiment are crucial problems. Raman spectroscopy and field effect characterization are two of the most common methods that are used to obtain information about the quality of a graphene layer, the number of the graphene layers, the type of doping and impurities. Those two methods are ideal because they are nondestructive, fast, and relatively simple.

2.1.2.1 Raman Spectroscopy

Raman spectroscopy is one of the most sensitive methods to characterize graphene. This method provides a rapid and nondestructive measurement of graphene. The Raman effect occurs if an electromagnetic wave is absorbed by the material. It results in the excitation of rotational or vibrational states of atoms in the material. While some part of the input electromagnetic wave is stored as atomic rotations or vibrations, another part of the energy is emited as scattered photons. This is the origin of the energy shift in Raman spectrum. The measurement of a Raman spectrum results in several peaks that correspond to certain properties of the observed material. The primary features in such a spectrum are the G-band, the D-band and the 2D-band, beside other Raman modes such as the D'-band and D+G-band [33]. The positions of each structure are approximately at 1350 cm^{-1} for the D-band, at 583 cm^{-1} for the G-band, at 2680 cm^{-1} for the 2D-band, at 1620 cm-1$for the D'-band, and 2947 cm^{-1}$ for the D+G-band [34]. The positions in the Raman spectra are affected by the number of the graphene layers and the existence of defects or impurities. The ratio of the G-band intensity to 2D-band intensity can be used to determine the number of the graphene layers. If the 2D-band is more intense than the G-band, it shows that the sample consists of only few layer of graphene. On the other hand, if the G-band is much more intense and sharper than the 2D-band indicating that the sample is multilayer graphene [35]. Impurities or surface charges in graphene layer causes the G-band to split into two structure, G-band and D′-band. The D-band correspond to defects and disorders in the graphene structure. In good quality pristine graphene, the D-band and D′-band do not appear, only G-band and 2D-band that dominate the spectrum.

2.1.2.2 Field Effect Characterization of Graphene

The graphene field effect characterization is carried out by applying a voltage bias to the gate of a graphene device (fig. 2.3). The resulting electric field penetrates the graphene and attracting more carriers from the substrate to graphene layer. Therefore, the magnitude of the field dictates the value of the Source-Drain (SD) current passing through the graphene layer due to the electric-field-dependent carrier concentration. The lowest current is observed from the particular voltage at which the carrier is minimum. The amount of the lowest current is called the Dirac point. For pristine graphene, the position of the Dirac point is at zero voltage. The other parameter besides current that is also used for field effect characterization is

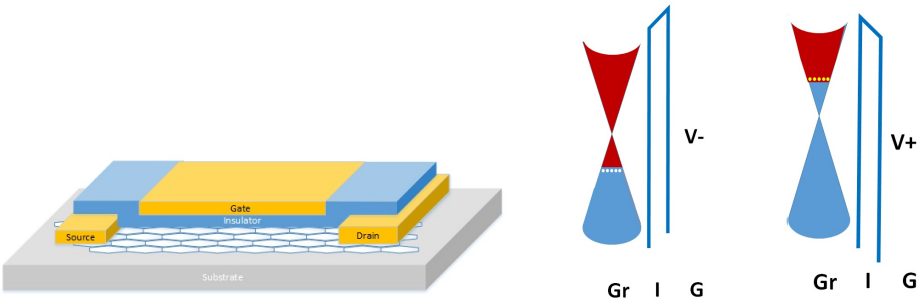

(a) (b) (c)

Figure 2.3: (a) Field effect graphene, the Source-Drain (SD) current passing through the graphene layer depends on the potential of the gate. (b) Field effect graphene energy band. Gr for the graphene energy band, I for the Insulator energy band and G for the gate. The blue (red) region represent the valence (conduction) band of graphene layer. Negative voltage of the gate attracting positive carriers to graphene layer. White dots represents the holes (c) Positive voltage of the gate attracts negative carriers to graphene layer, yellow dots represents the electrons.

resistance. In contrast to a current measurement, the Dirac point is reached if the resistance is at its maximum. Different positions of Dirac point mean that graphene has different properties e.g. doping, heating, and pumping.

The Dirac point shifts to positive or negative voltages depending on the type of doping. The positive (negative) position of the Dirac point shows that the type of doping is p-type (n-type) [36] (fig. 2.4.a). The higher the doping concentration, the further the shift from zero voltage (fig. 2.4.b). Shifting of the voltage of the Dirac point is often not be followed by a change in the maximum resistance. This means that graphene is not affected by a change other parameters besides the doping. The gradient of the Resistance-Voltage (R-V) graph sometimes also follows a shifting of the Dirac point position. A graph with smaller gradient indicates that the doping concentration is higher [37]. By comparing the R-V graph of graphene as function of time, the transformation of graphene due to doping and the corresponding change of the electronic properties cam be analyzed. Furthermore, with this method, the reproducibility of a graphene device is readily checked by comparing the R-V characteristic of one sample to another.

The shift of the Dirac point to zero voltage is observed because graphene already has been doped. To bring graphene in a neutral condition, the unintended doping should be compensated with opposite carriers that is attracted by electric field. The value of maximum resistance can be shifted because the minimum number of carrier in the material depend on pressure, temperature, and the number of defects.

Measurement of graphene properties can also be carried out by monitoring the change of resistance without biasing the back gate. This type of measurement works as simplified R-V characterization with zero back-voltage bias. The change of resis-

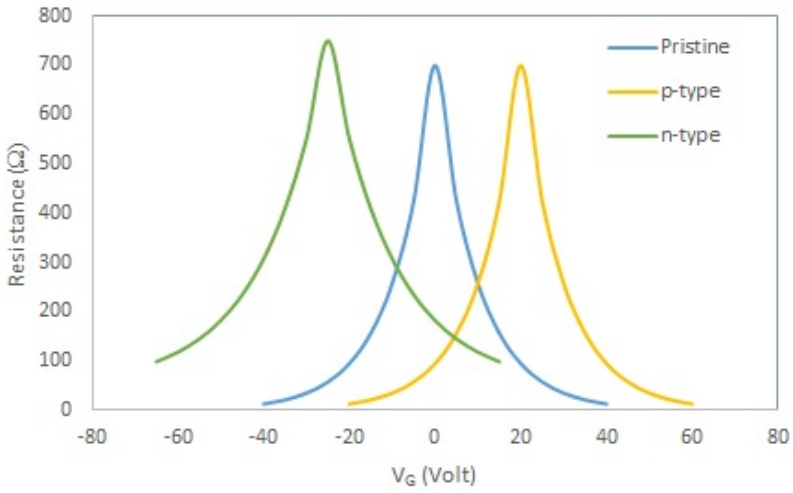

(a)

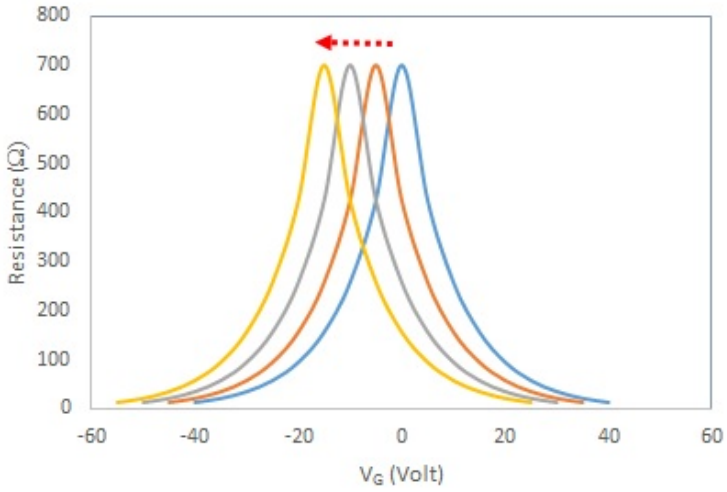

(b)

Figure 2.4: (a) The resistance as function of gate voltage for three type of graphene. The blue graph represent a prinstine graphene that has Dirac point at 0 Volt. The green graph shifted to the left compared to pristine graphene represents p-type of graphene. The defects creation can shift the maximum resistance to a higher resistance value (b) The shifting of Dirac point as the increasing of doping level in a p-type graphene. Higher doping concentration is shown by red arrow. [37]

tance in graphene indicate a certain change of electronic properties of graphene. The decrease of resistance corresponds to increase of the carrier concentration. However, the increase of resistance corresponds to a decrease of the carrier concentration and the creation of defects. The doping concentration can be changed in course of an experiment by change of pressure, change of temperature and exposure to radiation.

2.1.3 Radiation Hardness of Graphene

The creation of defects by impinging ions in graphene depends on the charge, kinetic energy and density of ions [27, 18, 38]. The larger the charge, the larger the probability for ions to cause significant damage in graphene. On the other hand, every ion with a certain charge has a range of kinetic energy to create damage in the graphene layer. The energy deposited in a graphene layer is smaller for an ion with higher kinetic energy due to the smaller cross section. Helium ions (alpha particles) do not remove any carbon atom from a graphene layer if the kinetic energy is only a few eV or above 10 keV [39].

Electrons, protons, and ions with relatively low kinetic energies can penetrate graphene without leaving any significant damage in the graphene structure [27, 40]. Most defects in the graphene layer are not caused by a direct interaction between graphene and the ion because of the negligible cross section of that interaction [41]. However, the defects originate from the indirect effect of electronic excitations [27]. The electronic excitations energy creates a local annealing effect with radius few nanometers, and its temperature can reach more than 800 K [42], a temperature that is enough to create defects in the structure of graphene. However, graphene also has very high thermal conductivity, therefore the heat energy can be rapidly distributed. Hence, graphene suffers an insignificant number of defects from the electronic energy.

2.2 Other Two-Dimensional Material

Transition metal dichalcogenides can be fabricated as a two-dimensional (2D) material as graphene. These materials are attractive because some of them are semiconductors with a direct band gap. Molybdenum disulfide (MoS_2) is transition metal dichalcogenide that attract more attentions than other 2D transition metal dichalcogenides such as WS_2, WSe_2, $MoSe_2$, NbS_2, and $NbSe_2$. MoS_2 is classified as a two-dimensional semiconductor with 1.8 eV direct band gap [43]. The existence of the bandgap in MoS_2 makes this it easier to use this material for electronic devices based on semiconductor technology. Some devices require a band gap in its channel such as Field Effect Transistor (FET), one of the most important devices in electronic today. The band gap is required to switch the device from an on to off-state. If there is no band gap, it is difficult to realize an off-state. In off-state, the device is in a reverse bias condition of Positice-Negative (P-N) junction . If the material has no band gap, a significant leakage current is easily triggered by tunneling.

However, the overall electronic and mechanical properties of MoS_2 cannot compete with the superior mechanical and electrical properties of graphene. For an application as ion detector, the ion should pass through the 2D material in perpendicular direction. Unfortunately, even protons that has low energy (0.7 eV) cannot penetrate a single layer MoS_2. On the other hand, the protons can penetrate a single

layer of graphene with generating no atomic-scale defecs [44]. MoS_2 properties also show aging effects while graphene properties remain stable while storing during several weeks [27]. Furthermore, under swift heavy ion radiation of 1.14 GeV U^{28+} ion, MoS_2 Field Effect Transisors (FET) show a severe change of their characteristics, while the graphene FET shows an acceptable degradation. Moreover, a graphene FET is still in operational even in high-fluence 4 x 10^{11} ions/cm^2 radiation. Thus, due to the robust and permeable properties against particle irradiation, graphene is a more suitable choice of 2D material for the ion detector application is graphene.

2.3 Time of Flight Detector

Every heavy ion that hits a layer of matter deposits some part of its kinetic energy in the material. The maximum energy that can be transferred by an ion with a kinetic energy E and mass m to an electron with mass m_0 in a single collision is $4Em_0/m$ [45]. Because the mass of the ion is much larger than the mass of an electron, it takes many collisions to decrease the kinetic energy of an ion significantly. If the absorber is very thin, the reduced velocity, straggling and angular spread of the ion is small.

Some energy loss of a particle is expected when it passes through the detector. When an ion is passing through the layer of detector, the electric field of the ions excite the e-h pair in the layer. Attracting those electrons and holes to electrodes of the opposite polarity allows the detection of electronic signals. By using two detectors separated by a certain distance, the measurement of the time for the ions to travel the distance is possible. This detection method is called Time of Flight (TOF).

The TOF is needed to measure the velocity of an ion passing through the two separated layers of detector. A magnetic field that works uniformly through out the trajectory of ions deflects the direction of ions direction, so that an ions with particular charge and mass have a definite path. The simplified process of ion detection is shown in fig. 2.5. The magnitude of the magnetic field is tuning the bending radius of the ion trajectory. The relation between the magnitude of the magnetic field and radius of the trajectory is called magnetic rigidity (R). By a simple calculation of Lorentz and centripetal force, shown in equation 2.1, information about the mass of the isotope ion can be obtained.

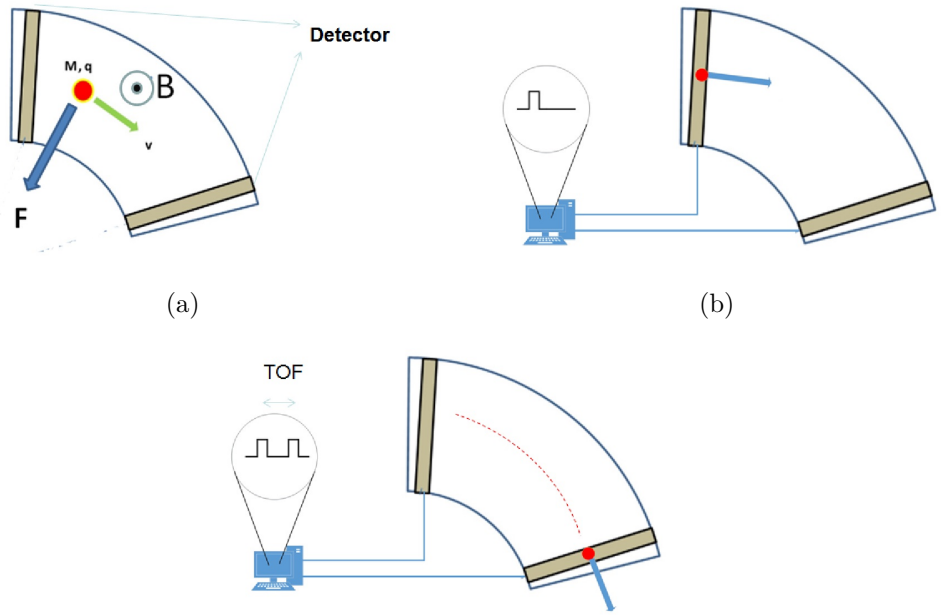

(a) (b)

(c)

Figure 2.5: Time of Flight Detection Method [46]. (a) An ion with mass m and velocity v is passing a TOF detector. The ion is represented by red dot, the magnetic field that directs inside the plan is considered uniform through out the detector area. The ion is attracted to the inner side of the trajectory by the magnetic field. (b) The ion passing the first layer of the detector, so it generates the first signal that is processed by a computer system. (c) The ion is passing the second detector and generating the second signal. By these two seperated signals, the computer system can calculate the time between both signals.

$$\begin{aligned} F_{Lorentz} &= F_{Centripetal} \\ Bqv &= \frac{mv^2}{\rho} \\ B\rho &= \frac{mv}{q} \\ m &= \frac{(B\rho)q}{v} \\ m &= \frac{Rq}{v} \end{aligned} \tag{2.1}$$

B is the magnetic field, m is the mass of ion, q is the charge of ion, v is the velocity of ion, ρ is the radius of ion trajectory, and R is magnetic rigidity.

2.4 Semiconductor Detector

For a understanding how the ion detector works, a silicon detector can be a good representative of a conventional ion detector. A silicon detectors are well-established particle detectors used extensively in the nuclear physics. Silicon is a semiconductor material with an energy gap 1.115 eV at room temperature [45]. The advantage of using a silicon detector rather than another type of standard particles detector, such as a gas-filled detector is it has relatively a low ionization energy. The ionization energy is minimum energy that is needed to create an electron-hole (e-h) pair in a material. The ionization energy for silicon detector is 3 eV, compared to the ionization energy in gas-filled detectors of about 30 eV. The detector is exposed to an electric field of reversed bias P-N junction to attract electron-hole. The electric field is generated only in the space charge region (SCR).

A signal that come from the generation of electron and hole (e-h) pairs by ionization process is the source of information that an ion is passing through. The main target of designing a detector is optimizing e-h generation and separation to produce a high quality signal. The silicon detector is designed as reverse bias Positive-Negative (P-N) junction for separating generated hole and electron. The P-N junction is fabricated by giving different type of doping to the opposite side of a semiconductor material vertically. By applying reverse bias condition to the semiconductor, leakage current could be minimized. The reverse bias condition produces high electric field to attract hole and electron to the opposite direction. This mechanism is avoiding recombination of generated electron and hole that result in loss of the ion footprint.

Making a fully depleted structure of Silicon is a critical task to optimize the collection of the electron-hole pair, because it results in SCR in its entire structure. In p-n junction, a lowly doped semiconductor produces a wider SCR and the highly doped semiconductor produces a narrower SCR. The silicon detector is fabricated to form three layers of different doping for resulting a fully depleted region. The layers are a stack of thin highly doped n-type (p-type), a thick low doped p-type (n-type) and thin highly doped n-type (p-type) silicon as shown in figure 2.6. When the ion is passing through the semiconductor detector, the electron is attracted to highly doped n-type and the hole is attracted to the highly doped p-type semiconductor. Because of both high doping regions are connected with electrodes with the opposite polarity, the attracted electrons and holes can be converted as electronic signals.

2.5 Design of Graphene Detector

As outlined above, graphene has outstanding electronic, thermal, and mechanical properties. This thin material allows ions with low energy pass through a layer of it without losing a lot of kinetic energy. Significant energy losses of ions in conventional detector result in the difficulties for the identification of an ion in e.g. a radioactive

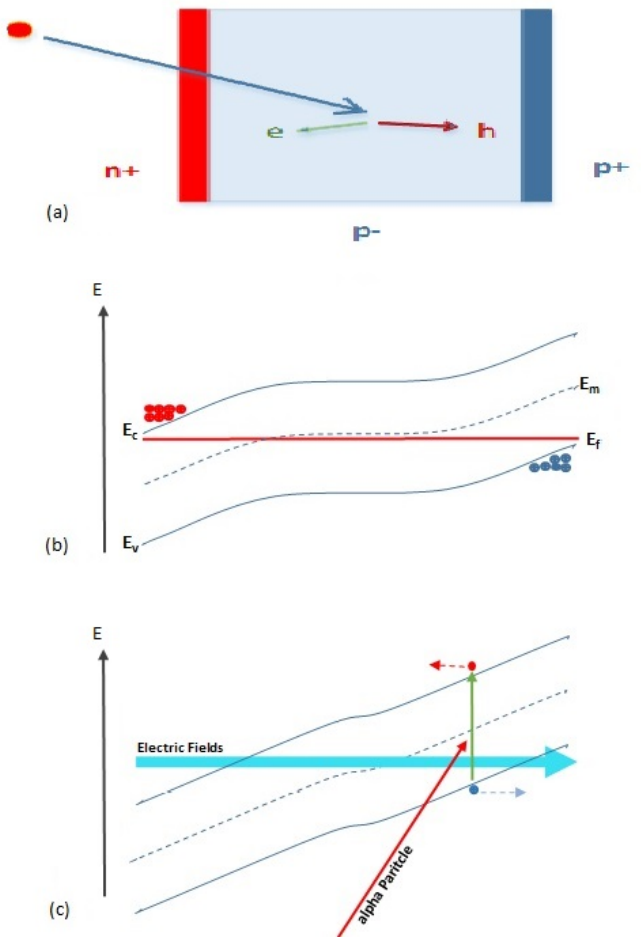

Figure 2.6: (a) n^+ and p^+ mean highly doped n-type and p-type semiconductor respectively. p^- means lowly doped p-type semiconductor. (b) The energy band of semiconductor detector without voltage bias. The red line represents Fermi energy (E_F) that level in neutral condition, red dots represent electrons and blue dots represent holes (c) Under reversed bias condition the energy band is a slope over all regions that indicate the existance of electric field everywhere. If alpha particles are passing through the semiconductor layer, the excited e-h pair is attracted to the opposite directions by the electric field.

beam that has been created in a nuclear reaction. On the other hand, the high electronic mobility is promising a fast response of graphene to a passing ion because the high electronic mobility result in a higher velocity of the carriers. Furthermore the mechanical robustness and the high thermal mobility gives graphene layer an exceptional radiation hardness. When ions penetrate a graphene layer, the high mechanical robustness prevents ejection of the carbon atoms and the high thermal mobility prevent thermal spike that could produce significant defects in the graphene structure. Based on these facts, graphene has potential to be a novel type of heavy ion detector. Therefore, in this thesis the possibility to use graphene as ion detector

is tested.

2.5.1 Graphene Ion Detector based on Electron-Hole Pairs Excitation

For resulting a signal, electron-hole generations is one of the possible mechanism that can be exploited for designing graphene detector. Electron-hole pairs generation in graphene is explained by the impact ionization. When ion passing through a graphene layer, the ion and graphene atom generate electron and hole pairs by impact ionization process. On the other hand, the recombination mechanism is occurred through Auger recombination process [47]. With zero band gap property of graphene, impact ionization should be easier to be generated even in low energy transfer. However, the absence of the band gap also give more chance to electron and hole pairs to recombine rapidly as well.

The electron-hole (e-h) pair generation and recombination rate depends on the e-h density and the temperature of graphene [47]. For graphene at room temperature, the generation rate can reach up to 10^{21} $cm^{-2}s^{-1}$ if the density of electron and hole is about 10^{1} cm^{-2}, however at that concentration the recombination rate is in the same order as the generation rate. If a higher concentration of the carriers is reached, the recombination rate overwhelms the generation rate. However, if the concentration of the carriers is lower, at about 10^{7} cm^{-2}, the generation rate can reach 10^{19} $cm^{-2}s^{-1}$; seven orders of magnitude larger than its recombination rate. Furthermore, e-h pairs generation is faster in lower e-h pair concentration while the time needed for recombination is order of magnitude longer than the generation time. From detection point of view, the recombination time in graphene is a crucial parameter note that in standard semiconductor (e.q. silicon or germanium) the recombination time is much longer than in graphene, typical time in a range 500 ps to 50 ns [48]. Graphene, on the other hand, at e-h concentration of 10^{11} cm^{-2} has a recombination time of about 1 ps and can reach more than 1 ns at an e-h concentration below 10^{9} cm^{-2} at room temperature [47].
There are two concepts about what kind of mechanism that can be used to build a graphene detector. First, graphene is doped to bulid a reverse P-N junction to imitate mechanism in silicon detector. If the ion is passing the graphene layer, it generates e-h pairs and produces a significant amount of current compared to leakage current, which can be detected. The second mechanism, a current is biasing to the graphene layer, when ions are passing through, the ion could disturb the current, and the change of current from disturbances could be measured.

The Positive-Negative (P-N) structure of graphene is built to produce a reverse bias device. With reverse bias, a high electric field throughout the graphene layer could be generated without resulting significant leakage current. The high electric field attracts electrons and holes in opposite directions and creates a current signal. Therefore, it is important to minimize the leakage current so that the signal can

be extracted. For a lateral structure, a single layer of graphene is doped on its two sides with a different type of doping.

On the other hand, in vertical structure, this P-N junction consists of two layers of graphene that have different doping with a thin insulator in between. The vertical design of the graphene detector allows for a perpendicular electric field in graphene that improves the number of free carriers. Furthermore, the vertical structure results in a uniform distribution of electric field throughout the graphene layer that could separated electron-hole pairs more efficiently.

The graphene that is used in our experiment is lateral graphene. The drawback of a large lateral graphene layer (about 1 mm x 1 mm in our structure) is that the distribution of the lateral electric field is not uniform. The strong electric field is only generated in the Space Charge Region (SCR), a region that most doped atoms are ionized. When the contacts are fabricated at the sides, the SCR is only generated in the center of the graphene sample, the rest of the graphene has no strong electric field to attract the e-h pairs. To turn the entire graphene surface into an SCR, lowly doped graphene could be used as bigger part of the junction. However, it also does not guarantee a significant leakage current could be prevented because without bandgap; the leakage current is likely to occur. Therefore, the separation process of e-h is possibly inefficient or even fail in such structure. On the other hand, in the vertical p-n junction, one layer of graphene has a single type of doping. It behaves like a metal that produces a negligible potential drop on it the entire layer. Such a vertical structure can generate an SCR on the whole surface of graphene because the distance between the two types of graphene is relatively close. Therefore, the separation of electrons and holes to produce signal can be more efficient in a vertical structure than in the a lateral P-N junction graphene detector.

2.5.2 Graphene Ion Detector based on Electron Scattering from the Substrate

Poly(methyl methacrylate) (PMMA) is a thin material that is commonly used for supporting substrate of graphene during transfer process. The elastic properties of this material give minimum probability to result in severe damages in a graphene layer. Besides, PMMA is also a positive tone resist polymer that is dissolved by developer after electron beam exposure. During the exposure, the electron beam results in inelastic scatterings in PMMA material that knock out several valence electron in PMMA structure. The removal of the valence electrons also means the scission of atomic bonds of the resist. Eventually, the absence of the atomic bonds in the polymer chains gives access for developer to binding with the resist single monomer, and etch away the resist material. The scission process is also scattering of some valence electrons [49]. The first collision between electron beam to PMMA could result in elastic and inelastic scattering. The elastic scattering only deviate the electron direction without decreasing the electron energy. The inelastic

scattering releasing a valence electron and it scatter the valence electron to generate a secondary inelastic scattering and produce more electron. This process could be continues in many cycles depends on the absorbed energy.

The Ionizing radiation also results in such scission effect in a polymer structure [50]. Therefore, it is expected that during alpha irradiation the electrons that are excited in the PMMA could be deposited in the interface of graphene layer and detected as current signals. The graphene, in this respect, acts as a reservoir for those electrons that can deliver the accepted electrons to the electrodes.

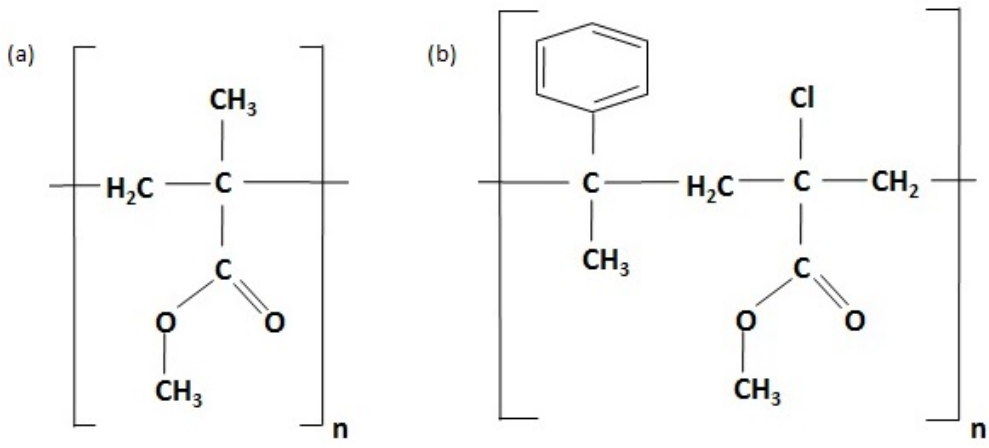

Figure 2.7: (a) The polymer structure of PMMA (b) The polymer structure of ZEP. The differences between both structure are the ZEP has Clorine group that substitutes the methyl and an additional hexagon structure of Phenyl side group in every unit of its monomer [49].

ZEP (1:1 copolymer of α-chloromethacrylate and α-methylstyrene), in the other hand, is also positive tone material that has the same main structure as PMMA except it contains side Phenyl group and a Chlorine group (fig. 2.7). Those two groups give ZEP more valence electrons that involve in inelastic collision than in the PMMA structure Table 2.1. More involved valence electrons means in every penetration of alpha particles throughout its layer, a bigger probability of alpha particles to scatter more electrons from the polymer structure. Therefore, ZEP is expected to produce signals more efficiently than the PMMA film.

Groups that the valence electrons significantly involve in inelastic collisions	PMMA	ZEP
Main-chain C-C bonds		
- Number of electrons per monomers	4	8
- Ionization energy (eV)	3.5	3.5
Side groups		
- Number of electrons per monomers	-	38
- Ionization energy (eV)	-	3.5
Other valence electrons		
- Number of electrons per monomers	36	40
- Ionization energy (eV)	16.52	16

Table 2.1: Comparison of PMMA and ZEP resist model for inelastic collisions [49].

3

Experiment Method

In this experiment, we want to study about the effect of irradiation of alpha particle on a graphene layer has namely, how the ion penetrates the graphene layer and the radiation hardness of graphene. In order to measure the stability and radiation hardness of graphene, the resistance of graphene at atmospheric air, under vacuum and under irradiation of alpha particles are measured. This data provides information about the change of the electronic properties of graphene during the pumping process and the irradiation of alpha particle. In this work, the resistance was measured between two points instead of four points. The correction due to four point contacts is significant for a material that has a resistance of less than 100 Ω. In this case the resistance of graphene is always higher than 400 Ω. Therefore, the resistance measurement is still valid. The second data about the energy and number of α-particles is provided by the data acquisition system (DAQ). The DAQ with support from a silicon detector and appropriate electronics can provide information about the number, and the energy losses of of α-particles that penetrate the graphene layer. In order to examining signals that is produced by graphene during alpha irradiation, the signals are analyzed by an high precition oscilloscope.

An experiment that is involving heavy ions with energy lower than Coulomb barrier (<8 MeV) should be carried out in accelerator. For the purpose of development of a material for a novel detector, a simpler ion such as α-particle is utilized. To study the effect of the irradiation on the electrical properties of graphene, α-particles from a radioactive source used in this experiment has activity of 150 nCi ($5.55x10^3$ decays/second). It contains three different isotopes Plutonium (^{239}Pu), Americium (^{241}Am), Curium (^{244}Cm) resulting in decacy that produces α-particle with energy 5.15 MeV, 5.48 MeV and 5.80 MeV respectively [51]. These three different α-particles energy also give the opportunity to compare each of the peaks during the measurements.

The experiment with graphene is carried out in two different environments, measurements were performed in ambient air with atmospheric pressure and under vacuum condition. Both conditions are at room temperature. The vacuum chamber is pumped by a roughing pump and a turbopump. With the roughing pump, a pressure can be reached below 1 torr, and combined with the turbo pump, a pressure can be reached below 1 μtorr. The setup for this experiment consists of the graphene, the alpha source, silicon detector, the vacuum chamber, electronics, and the data

acquisition system.

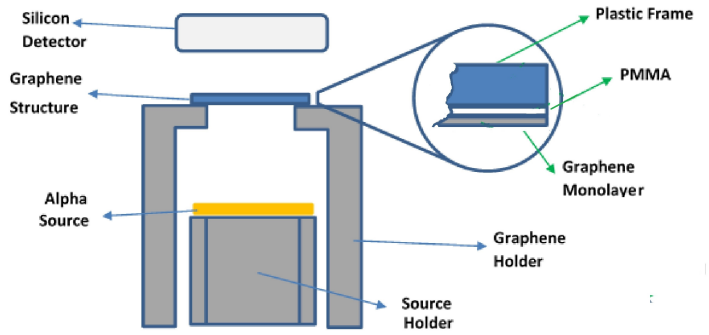

(a)

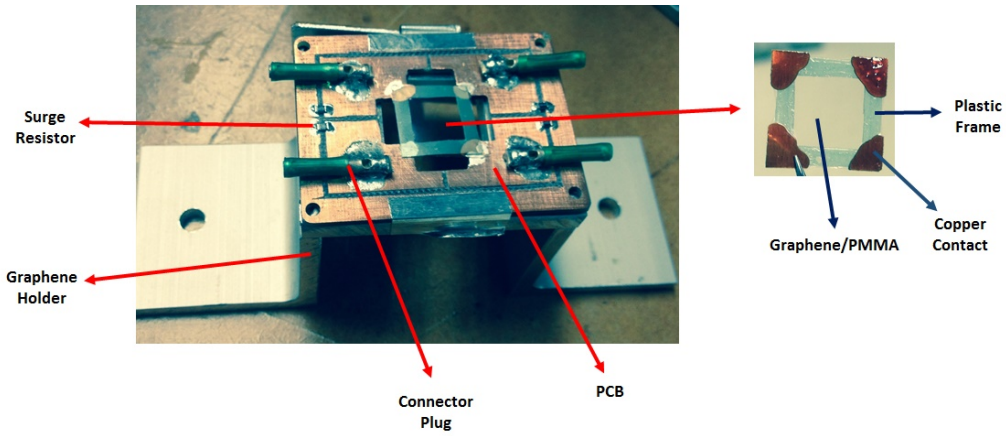

(b)

Figure 3.1: Experiment set-up. (a) The α-particles source, sample and semiconductor detector are parallel placed. The sample is consisted of three (four) layers: the graphene monolayer, PMMA, (ZEP) and plastic frame. (b)The holder is designed to prevent the shorting of the graphene contacts. Therefore, the top part of the holder is attached to PCB that is divided become four separate parts by trench. Morover, four surge resistances is applied to prevent voltage spike effect that might destroy the sample. The plastic frame is at the perimeter of the sample, therefore the alpha particles only penetrate graphene monolayer, (ZEP) and PMMA.

The arrangement of the set-up used in this experiment is shown in figure 3.1. During the measurement, all the instruments are put inside the chamber that has a shutter. The shutter is made form a few milimeters metal that can be closed and open immediately. If the shutter is closed, its position is in the middle between alpha source and graphene, therefore it prevents the exposure of α-particles to graphene. On the other hand, if the shutter is open, it is pulled back and α-particles can pene-

trates graphene layer. Furthermore, the shutter makes a precise time measurement can be obtained during the experiment. If the experiment of alpha irradiation effect toward the graphene layer is started, it can simply start timing after the shutter is opened for letting alpha particles penetrate the graphene. The distance between the α-particles source and semiconductor detector is kept to fix about 4 cm while the distance between the source and the graphene sample is about 2.5 cm. The short distance between the α-particles source and graphene is critial for the measurements in atmospheric pressure, due to the significant scattering of α-particles in air.

For this experiment, five samples were prepared for the measurements. The method for checking the effect of alpha irradiation was varied throughout the samples. The sample 1 was exposed by alpha particle in atmospheric pressure by opening the shutter directly from the beginning of measurement. On the other hand, the sample 2, the sample 3, the sample 4, and the sample 5 were exposed by alpha particle by opening the shutter after pumping and they reached a saturation resistance. Besides, additional steps were applied to sample 3 and sample 5. For the sample 3, the shutter is opened continuously then closed for two hours, under two conditions with and without the source of α-particles inside the chamber. For sample 5, two additional methods were applied. the first method, the shutter was closed continuously and then opened for two hours. In the second method, the shutter is opened continuously then closed for two hours. Both methods were carried out under two conditions, with and without the source of α-particles in the chamber.

A silicon detector is chosen to become part of the setup. A silicon detector is placed in the back side of graphene sample to measure the energy loss of the alpha particle in the graphene/PMMA structure. The energy losses of alpha particle can be measured by comparing the energy of alpha particles in two conditions, without passing through a graphene sample and after passing through a graphene sample. Furthermore, a semiconductor detector is utilized as a guide for canceling noise in signal detection with the graphene layer. The noises from the electronics devices in data acquisition system can be separated from the real signal because a semiconductor detector results in a significant amplitude of signal compared to the noises. By subtracting the noise that is recognized by the semiconductor detector, it is expected a clear signal produced by graphene layer can be recognized.

The silicon detector was biased with +35 V. Resulting in a leakage current of 0.11 μA. Biasing the detector leads to the leakage current give in the table 3.1. With increasing bias voltage, we expect a larger depletion layer in the semiconductor detector. The typical thickness of semiconductor detector is up to 2 mm and the resistance is about 5000 Ω [45].

For all of the measurements, data were collected for one-hour or for longer measurement they were scaling down to be one-hour. Every process of saving the data, the system provide information about the specific time when the process is executed. The period of a measurement can be identified by subtracting the time of last data collection with the first data collection then adding with the interval of last two

No.	Voltage (V)	Leakage current (μA)
1	5	0.06
2	10	0.09
3	15	0.09
4	20	0.10
5	25	0.10
6	30	0.11
7	35	0.11

Table 3.1: Leakage current in the semiconductor detector

data. The adding of interval from the last two data collection has the purpose for compensating the first data collection time that cannot be counted directly. By scaling down the all of the histograms to be 3600 s, the comparisons of the number of counts from different experiments can be carried out.

The energy of alpha particles detected by the silicon detector were plotted in histograms made by the ROOT program. The x and y-axis of the histogram correspond to energy and counts of the alpha particles, respectively. All of the histograms (except that for sample 1) in this report represent one-hour measurement and are set to span 4000 bins. This allows to compare the number of counts per energy bin for each histogram.

3.1 Graphene-Structure Fabrication

The grahenes sample used in this experiment were supported by two different film materials. Sample 1, 2, 3 and 4 were supported by a poly(methyl methacrylate) (PMMA) film, while sample 5 was supported by ZEP (1:1 copolymer of α-chloromethacrylate and α-methylstyrene) photoresist and PMMA. The size of each sample was 1.2 cm x 1.2 cm with a plastic frame as scaffold supporting the samples at the sides. The graphene samples, that initially came on a copper film were bought from Graphenea, Spain. Our collaborators (Prof. August Yurgens and Grigory Skoblin) transfered that graphene on the top of with wet etching transfer and the spin coating method.

Graphenea synthesizes the single layer graphene films using Chemical Vapor Deposition (CVD) method on a copper foil with thickness of 18 μm. The Raman spectra for these graphene show there are only two dominant peaks corresponding to the G-band, and the 2D-band [52]. The intensity of the 2D-band is higher than that of the G-Band corroborating that the samples are a single layer grahene. Moreover, the absence of a D-band indicates the absense of lattice defects.

To transfer the graphene from copper to PMMA are needed several steps. Initially, diluted PMMA is spin-coated on the top of graphene/copper with 1000 rpm for 1 minute. The diluted PMMA has a concentration of 4% and a molecular weight

of 950,000. The PMMA film needs to be cured at 160 ^{0}C for 5 minutes. After the PMMA has hardened, polyethylene terephthalate (PET) with a thickness about 100 μm is attached to PMMA to provide a solid supporting frame that prevents the film from breaking easily. The frame is attached to PMMA with glue that can withstand a wet environment. Before copper etching, some photoresist is deposited on the corner part of the copper film. The copper at the corner is needed to provide electrical contacts to graphene. To remove the copper, the stack of frame/PMMA/graphene/copper is immersed in Ammonium persulfate (APS) copper etchant solution. Afterward, the stack is rinsed with deionized water. The stack is put on a clean tissue until it becomes dry at room temperature. The photoresist film that cover the copper contacts need to be removed with acetone. Finally, the contacts of graphene/PMMA sample are attached to a copper board on the graphene holder attached with silver conductive glue (fig. 3.2.a).

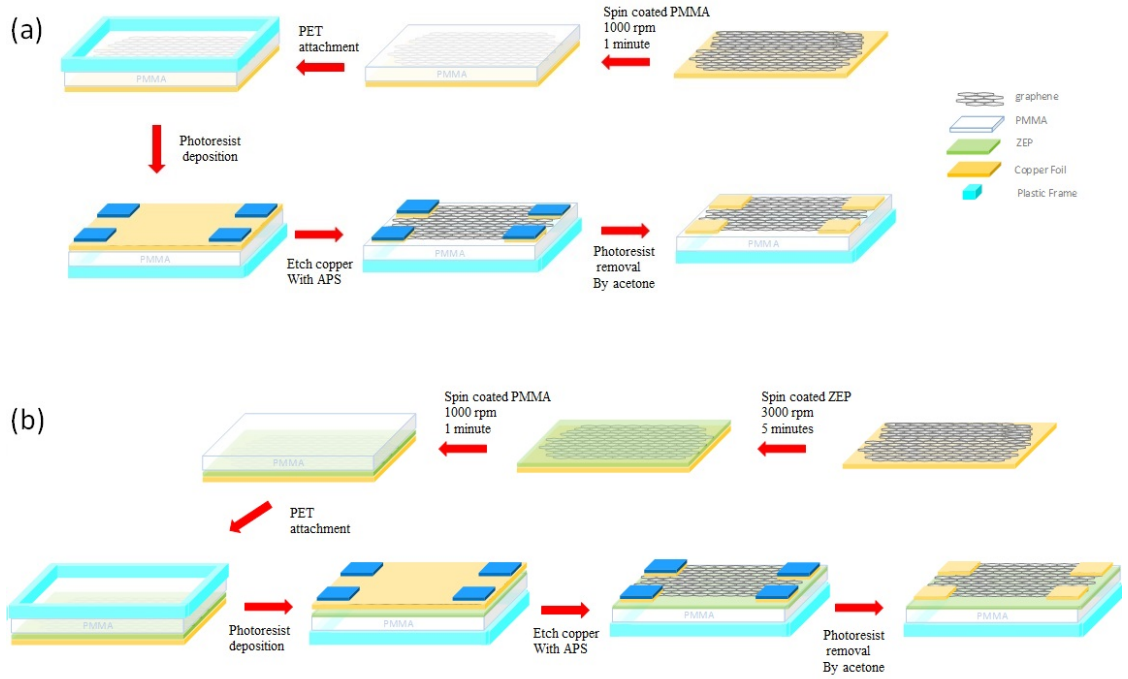

Figure 3.2: The transfer process of the graphene samples onto (a) a PMMA film (b) a ZEP/PMMA film.

The next type of sample is graphene doped with ZEP-520A photoresist. The fabrication of this sample followed the same processes used for creating graphene/PMMA but included an additional step in the begining. Undiluted ZEP-520A photoresist is spin-coated on the original graphene/copper at 3000 rpm for 5 minutes. After the ZEP has hardened, all process that are used for fabricating graphene/PMMA sample are followed (fig. 3.2.b).

3.2 Electronics and Data Acquisition System

Preamplifier and spectroscopy amplifier carry out the amplification and shaping of the signal into a Gaussian shaped pulse, while suppressing electronic noise. The timing signal are processed by timing filter amplifier followed by a constant fraction discrimination. The analog signal needs to be converted to a digital signal in Analog to Digital Converter (ADC). The constant fraction discriminator signal, timed appropriately with a gate and delay generator, provides a gate for the ADC. The flowchart of the system is shown in figure 3.3.

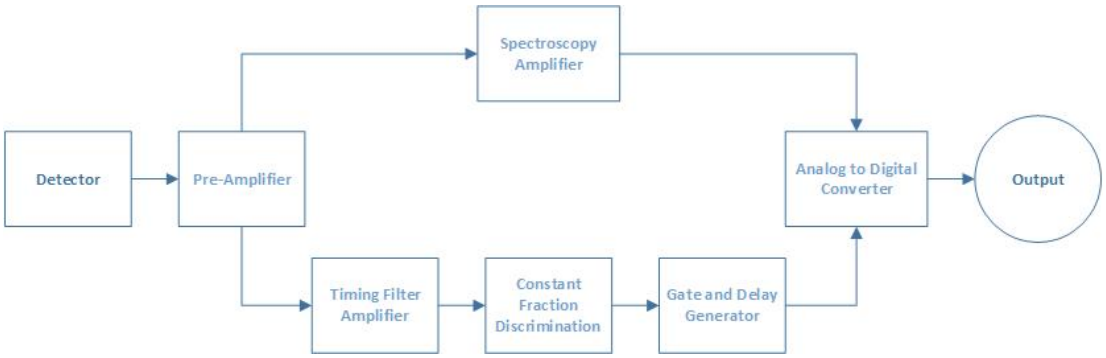

Figure 3.3: Flowchart of the data acquisition system

The preamplifier is an electronic device that collects the charge signal from the detector, convert it into a voltage pulse, and reduces electronic noise. The preamplifier should be as close as possible to the detector using a short cable connection. This reduces the contribution of the cable to the detector capasitance thereby minimizing noise. The signal from the preamplifier is sent to a spectroscopy amplifier and a timing filter amplifier.

The primary function of the spectroscopy amplifier is to magnify the signal amplitude of the preamplifier. The initial signal amplitude from the preamplifier is typically in order of some millivolt. The spectroscopy amplifier amplifies that signal to be in the range of 0.1- 10 Volt. Another important role of the spectroscopy amplifier is to shape the pre-amplifier signal into a positive Gaussian-shaped pulse that can be used by the Analog-to-Digital Converter (ADC).

3.3 Search for Graphene Signals

The number of alpha particle that produce isotropically in any direction by the alpha particle source is 5550 particles/s. However, the number of alpha particles that direct to the sample is about 25 particles/s. If every collision of the alpha particle with the sample resulting current from electron-holes generation, consequently the signal has period 40 ms. The precision of oscilloscope is down to a nanosecond. That precision guarantees the possible highest rate signal produced by the interaction of alpha particle measured precisely.

Every single alpha particle has charge +2e. If each of them produce a pair of electron and hole, they could produce 8 x 10^{-3} fA. However, the small ionization energy of graphene (<1 eV [53]) and scattered electrons from the supporting substrate are expected to result in larger current that is possible to be detected by our electronic devices. The electronic devices that are utilized for the detection of graphene signal are Preamplifier, Spectroscopy Amplifier and Timing Filter Amplifier. That devices are expected to be able to amplify the graphene signals and distinguish them form the noises, therefore the signals could be recognized in the osciloscope.

4

Results and Discussion

4.1 Measurement with Data Acquisition System

4.1.1 Setup and Fabrication Effect on Data Consistency

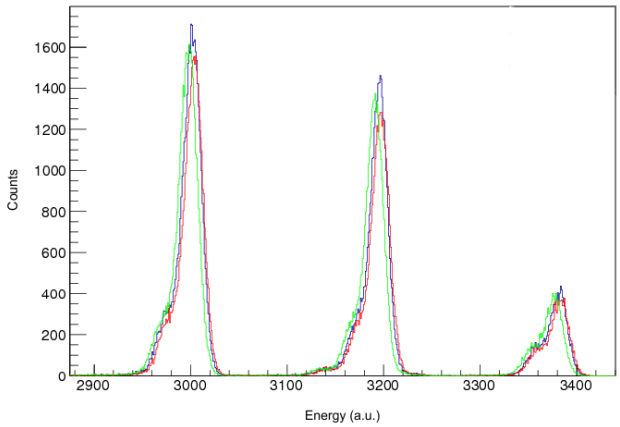

Figure 4.1: Histogram of three trials of setup rearrangement using the second PMMA sample.

All of the measurements using the data acquisition system is carried out at room temperature and vacuum condition except for sample 1 (Table 4.1). The sample 1 measurement is conducted in atmosphere pressure condition. For every measurement of a different sample, the setup that consists of a source of the α-particles, the graphene holder and the semiconductor detector need to assembled and disassembled. This procedure bears the risk moving the relative positions of those parts slightly. To study the influence of this, a PMMA sample is measured after three of assembly and disassembly steps. The results shows that the measurement is consistent with only give slight change of peaks position (fig.4.1). However, the measurement of the energy losses for the three trial is need to be carried out to know the reliability of the system for comparing one sample measurement to others.

The measurements of energy losses were carried out by comparing the peak positions with and without the sample in between the α-paticles source and the silicon detector. The peak positions correspond to the energy of alpha particles, which

are detected by semiconductor detector. By this method, energy that is lost in the PMMA sample could be calculated. Three peaks of the reference histogram, without the sample, relate to the initial energy of alpha particles from the source. The distance of shifted peak positions from reference histogram can be used to determine to the energy loss of alpha particles in the sample. The larger the shift of a peak position the larger energy loss of an alpha energy and vice versa. Although the histograms indicate only slight shifts, Table 4.2 shows the of the energy losses measurements of the second PMMA sample has a significant variation. This might be due to the slight tilting of the source and the semiconductor that create the significant variation.

Sample	**Supporting Film**	**Pressure**
Sample 1	PMMA	Atmospheric
Sample 2	PMMA	Vacuum
Sample 3	PMMA	Vacuum
Sample 4	PMMA	Vacuum
Sample 5	ZEP/PMMA	Vacuum

Table 4.1: The supporting film of all samples and the pressure condition during the measurement for each sample. All measurements were carried out at room temperature.

Peak	**Energy Losses (keV)**		
	1^{st} trial	**2^{nd} trial**	**3^{th} trial**
Peak 1	44	35	47
Peak 2	36	36	45
Peak 3	34	27	48
Average	**38**	**33**	**47**

Table 4.2: The energy losses of alpha particles that passing though second PMMA sample for three rearrangement trials of the setup.

The thickness of different PMMA film is also studied. The thickness of PMMA could be calculated using the information of stopping power. The stopping for α-paticles with energies of 5.15 MeV, 5.48 MeV and 5.80 MeV are $10.044x10^2$ MeV/cm, $9.607x10^2$ MeV/cm, $9.236x10^2$ MeV/cm respectively [54]. Four dummy samples were prepared for these measurements. The first two were made with 50 μm copper foil, and the rest with 25 μm copper foil. the result (fig. 4.2) shows a significant energy loss in PMMA.

Although all of the PMMA films are fabricated using the same technique, we found that there is a significant variation in their thickness. By averaging the results for three peaks (Table 4.3), the thickness of the first, second, third and fourth PMMA

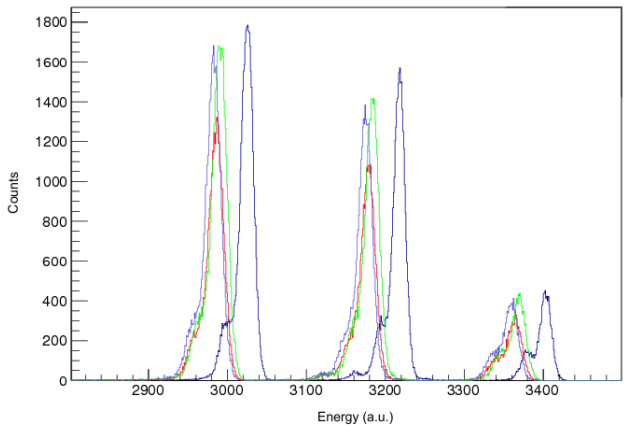

Figure 4.2: The red, green and light blue histogram correspond to first, third and fourth PMMA samples respectively. The blue histogram is reference.

Peak	**PMMA 1**		**PMMA 2**		**PMMA 3**		**PMMA 4**	
	E_l (keV)	**t (nm)**	**E_l (keV)**	**t (nm)**	**E_l (keV)**	**t (nm)**	**E_l (keV)**	**t (nm)**
Peak 1	68	670	44	440	66	662	75	748
Peak 2	65	680	36	380	64	664	74	771
Peak 3	67	720	34	370	68	739	68	739
Average	**67**	**690**	**38**	**397**	**66**	**688**	**73**	**753**
N_α (%)	**82.9±0.6**		**107.9±0.7**		**99.4±0.7**		**101.9±0.7**	

Table 4.3: The energy losses (E_l) and the number (N_α) of α-particles that are passing through the four PMMA samples with respect to the reference measurement. The estimation of the thickness (t) of PMMA samples are calculated with help of the stopping power information .

film are 690 nm, 397 nm, 688 nm and 753 nm, respectively. The third and fourth PMMA samples on top of a 25 μm copper foil shows the relatively uniform thickness compared to PMMA on top 50 μm copper foil.

The total number of the counts in an one-hour measurement is in the order of some tens of thousands. Therefore, the statistical errors for all measurement are always less than 1%. But for the PMMA measurements, it shows that the number of the passing α-particles for first PMMA sample is significantly smaller than the amplitude of other PMMA samples. On other hand, the number of the passing α-particles for the second and the fourth PMMA samples are more than 100% of that of the reference measurement. The problem might be caused by a shift of the setup positions or systematic error in the data acquisition system.

The source, the sample, the hole of sample holder and semiconductor detector could deviate slightly between different samples. The most possible shift is the relative lateral position of the setup, because the horizontal position is arranged manually. However, the contribution of a possible lateral shift of the setup relative

position is not significant for the total number of detected α-particles. On the other hand, during rearrangement the vertical position of the setup is expected to be constant for each measurement, except for the semiconductor detector. There is a possibility for the semiconductor detector to move slightly from its holder during the rearrangement. Based on solid angle calculations, a slight vertical movement of the setup results in a significant change of the detected number of α-particles. A 1 mm vertical shift results in about 10% fewer detected alpha particles.

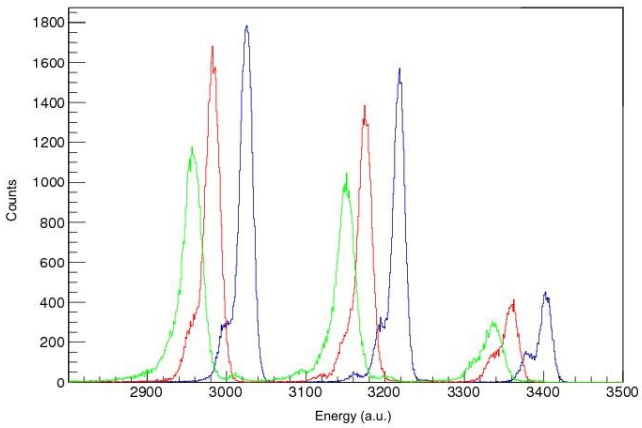

Figure 4.3: The green histogram correspond to ZEP/PMMA sample, the red histogram corresponds to PMMA sample and the blue histogram is the reference.

The ZEP/PMMA sample (fig. 4.3) shows that the energy losses of alpha particles in that sample are bigger than the energy losses in the PMMA sample (fig.). The greater energy losses in ZEP/PMMA is expected because the sample contains a PMMA film that has about the same thickness as the PMMA in the other dummy samples. The energy losses in the ZEP/PMMA sample is shown in Table 4.4. Unfortunately, a reference for the stopping power of alpha particles in ZEP film could not be found. However, the setup used for the fabrication of the film limits the maximum thickness of the film to 1 μm [59]. Therefore, if the third PMMA sample are choosen for reference, the ZEP film should has thickness less than 312 nm. If the stopping power of ZEP film is the same with the stopping power of PMMA film, the thickness of average of ZEP/PMMA is 1213 nm and the thickness of the ZEP film itself is 525 nm. The thickness of the film is exceeding the limit. Therefore the most possible condition is stopping power of ZEP is significantly larger than the stopping power of PMMA film.

4.1.2 Graphene under Alpha Particles Irradiation

For first sample (fig. 4.4), most of the alpha particle is absorbed by interaction with the air at atmospheric pressure. The two peaks correspond to alpha particles with energies of 5.48 MeV and 5.80 MeV. The third peak that corresponds with energy

Peak	PMMA 3		ZEP/PMMA	
	$\mathbf{E}_l$ (keV)	**t (nm)**	$\mathbf{E}_l$ **(keV)**	**t (nm)**
Peak 1	66	662	120	**1194**
Peak 2	64	664	114	**1184**
Peak 3	68	739	117	**1261**
Average	66	668	117	**1213**

Table 4.4: The energy loss (E_l) of third PMMA and ZEP/PMMA sample that correspond to each peak of α-particles energy. The table shows the thickness (t) of the ZEP/PMMA film if the stopping power of the ZEP film is the same with the PMMA film.

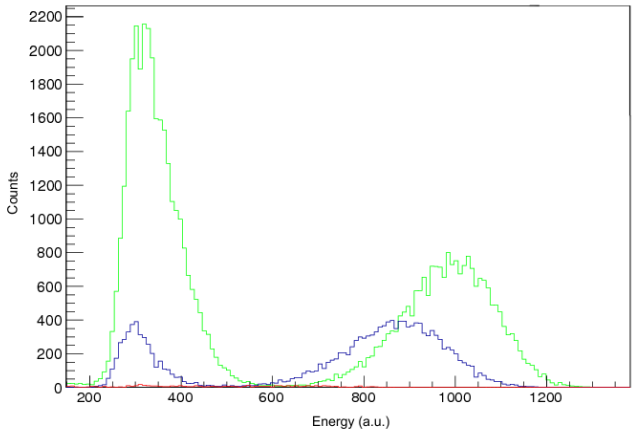

Figure 4.4: The green histogram corresponds to α-particles passing 4 cm of air and the blue histogram corresponds to α-particles penetrate sample 2 at atmospheric pressure.

5.15 MeV is not visible. The disappearance of this third peak shows that the number of absorbed alpha particles in air is significant. Therefore, the α- particles that are passing through sample 1 layer is only 29.8±0.4 % compared to the reference. The total energy that is lost in the graphene sample is difficult to calculated at atmospheric pressure because the alpha particles pass three layers of matters. The first is air for along 2.5 cm from source to the graphene structure. The second is graphene sample. The third is again air for 1.5 cm from graphene to the semiconductor detector. Thus, the measurements are best carried out under a vacuum to avoid losing some part of alpha particles in air.

The measurement using sample 2 (fig. 4.5), sample 3 (fig. 4.6) and sample 4 (fig. 4.7) were carried out in vacuum. The reference histogram shows all three peaks with narrower width because of no energy straggling in air. The energy of α-particles that is deposited in the samples are shown in Table 4.5. α-particles can deposit the energy in the graphene layer or the substrate film. However the energy that deposited in graphene layer cannot be acquired directly from the energy

Peak	Energy losses in the sample (keV)			
	Sample 2	**Sample 3**	**Sample 4**	**Sample 5**
Peak 1	46	44	49	91
Peak 2	40	40	48	88
Peak 3	35	40	46	87
Average	**40**	**41**	**48**	**89**
N_α (%)	74.0±0.4	57.8±0.4	115.2±0.8	100.3±0.7

Table 4.5: The energy losses of α-particles and number of α-particles (N_α) that are passing through the graphene samples.

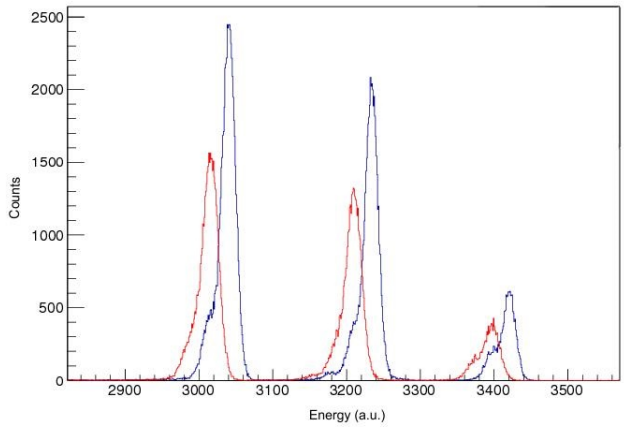

Figure 4.5: The red histogram correspond to sample 2 and blue histogram corresponds to the reference.

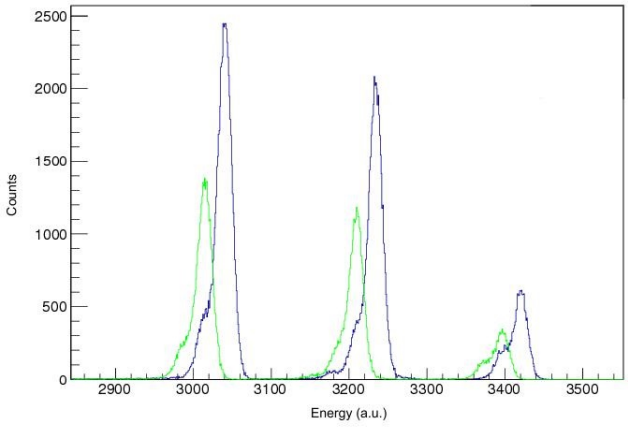

Figure 4.6: The red histogram correspond to sample 3, and blue histogram corresponds to the reference.

losses of α-particles. The deposited energy of α-particles in graphene/PMMA and graphene/PMMA/ZEP samples is always lower than that in the dummy samples, except for second PMMA sample. This shows that there is a tendency of the PMMA

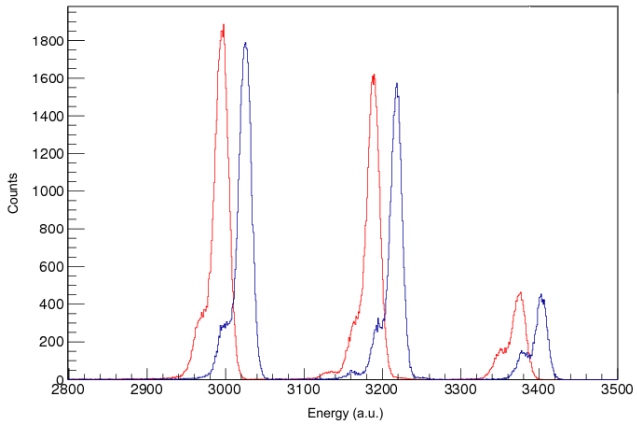

Figure 4.7: The red histogram correspond to sample 4, and blue histogram corresponds to the reference.

and ZEP films that are spin-coated on the top of graphene samples are thinner than those that are spin-coated on the top of copper foils. However, the deposited energy of α-particles can be indicated with other parameters. if there is part of the energy that is deposited in the graphene layer, it could be damaged structure of graphene atoms or e-h pairs could be excited. The excitation of e-h pairs can be detected by the observation of electronic signal and the increasing the resistance could indicate changes in the structure of graphene. On the other hand, the deposition of energy in the substrate film could lead to decrease of resistance because PMMA behaves as p-type doping for graphene. Because of the effect of energy depostion in graphene and substrate film are overlapping, the change of the resistance cannot be concluded comes from merely energy deposition in either layer.

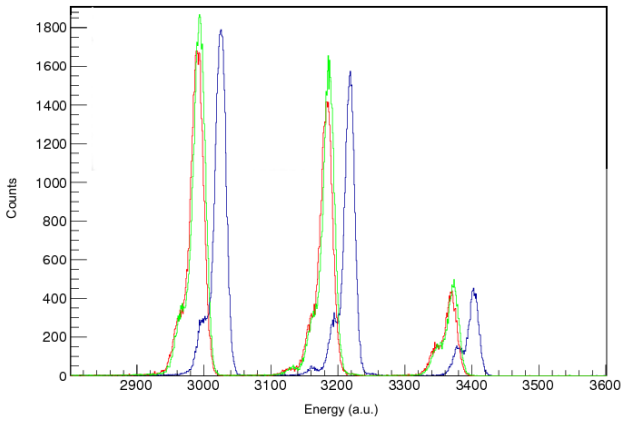

Figure 4.8: The red, green and histogram correspond to third PMMA, sample 4 and reference respectively.

The figure 4.8 shows that the peak positions of sample 4 are almost the same with peaks position of the third PMMA sample. That means energy is mostly deposited

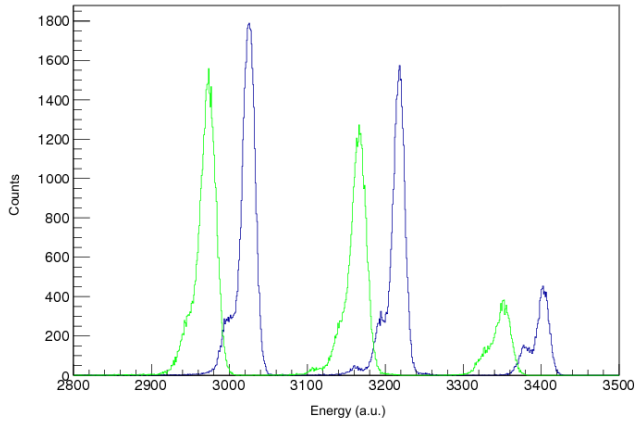

Figure 4.9: The red histogram correspond to sample 5 and blue histogram corresponds to the reference

in PMMA instead of the graphene sample. The PMMA sample is more than three order of magnitude thicker than a single layer graphene so this is expected. The histogram of sample 5 (fig. 4.9) that has an additional ZEP film shows a further shift compared to the other sample. Therefore, for sample 5 the most energy is deposited on the supporting film as well.

4.2 Resistance Characterization

The characterization of graphene using a resistance measurement in the absence of an electric field results in low carrier concentration in the graphene layer. However, the low level of carriers is also an advantage because it produces higher generation rate for e-h pairs, while the recombination rate stays low. The measurement is conducted using five samples. As described before, one side of graphene is attached to the supporting film while the other side is free to interact with ambient environment. All of the measurements were carried out at room temperature. For experiment using the second to fifth sample, pumping down to a 10^{-6} torr vacuum is done. The pressure environment (fig. 4.10) shows a linear decrease with the time on a logarithmic scale. The resistance characterizations of graphene were mostly carried out after several hours of pumping, when the resistance of graphene is already stable. Therefore, most of the measurements were conducted at a pressure of a few µtorr.

A measurement at 0.68 torr shows no change in the resistance of sample 5 under irradiation of α-particles. By opening and closing the shutter, the resistance measurement does not show any significant difference of its trend as typically shown in the lower pressure measurements. At higher pressure, the particle in the air is still abundant. Consequently, most of the alpha particle is damped by the air as shown in sample 1 experiment. Hence, reaching the lowest possible pressure is important to acquire clear conclusion about the interaction of graphene with alpha particles.

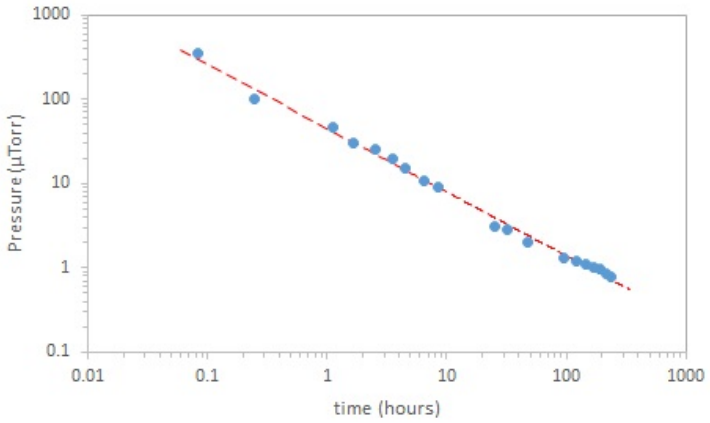

Figure 4.10: The rate of pressure change of vacuum chamber during pumping.

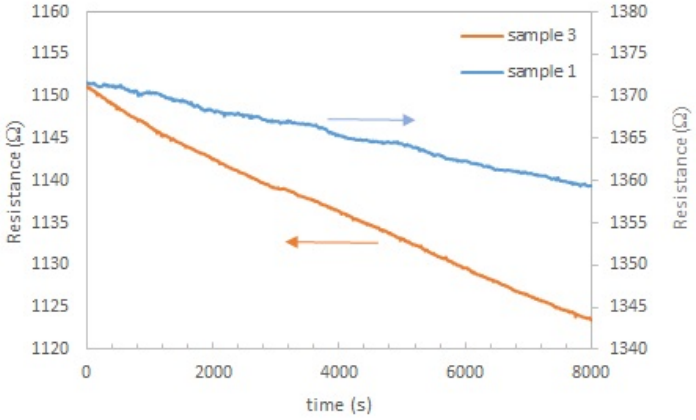

Figure 4.11: Resistance of sample 1 and 3 in the open-air condition.

For some cases, before the experiments started, graphene samples are stored without any enclosed container in a room with normal air circulation. This "open-air" condition indeed changes the electronic properties of graphene. Decreasing of the resistance in that open-air environment happens continuously for several days with the gradient decreasing as well (fig. 4.11). The molecules in the air, primarily oxygen and water vapor are acting as doping. Longer exposure time creates more carriers. More carriers in graphene produce a higher current that also means lower resistance. The decrease of the resistance gradient is a result of a lower rate of doping during the time of measurement.

When graphene is put in an enclosed chamber, the resistance is increasingly consistent with that of the sample under atmospheric pressure (fig. 4.12). This is opposite to what is observed in open-air. The decrease of the graphene resistance is also observed when graphene is stored in a chamber with an opened lid ((fig. 4.13), (fig. 4.14)). Other parameters, such as the impact of light irradiation is not the origin of this phenomenon. When the sample is kept inside the chamber and

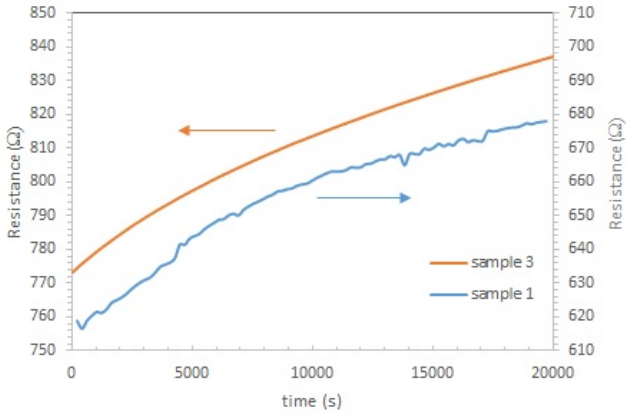

Figure 4.12: Resistance of sample 1 and sample 3 inside the chamber under atmospheric pressure

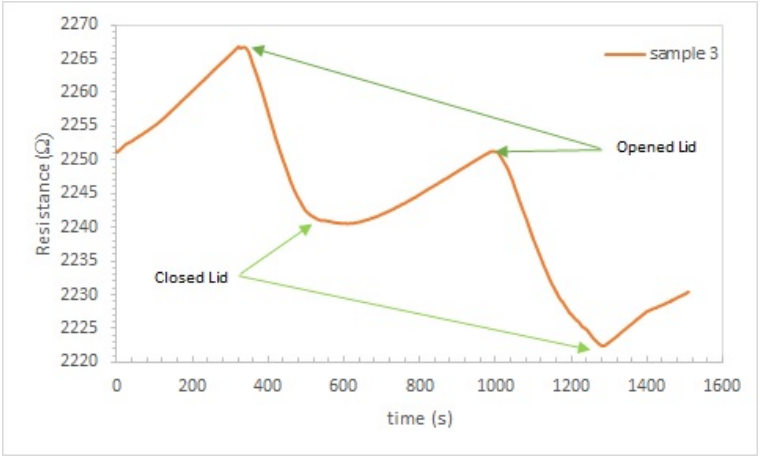

Figure 4.13: Resistance of sample 3 during opening and closing the lid chamber.

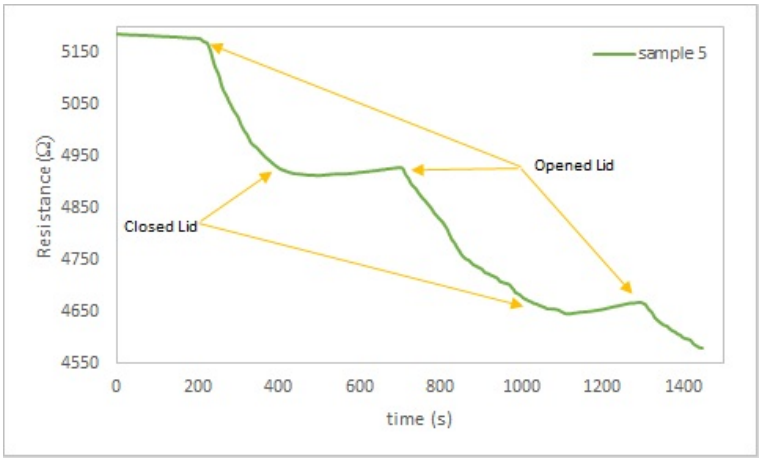

Figure 4.14: Resistance of sample 5 during opening and closing the lid of chamber.

a flashlight that is switched on is put inside, the observation is still reproduced

consistently while the chamber is opened and closed repetitively. This might be because the composition of the gas and humidity in the vacuum chamber are different from the composition of the gas in open air. For any sample, the condition inside the chamber makes the resistance of graphene to increase. This increase continues slowly for several days.

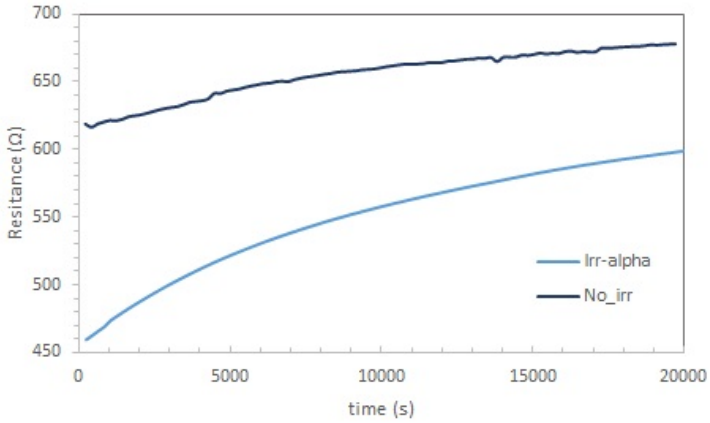

Figure 4.15: Resistance of sample 1 with and without alpha particles irradiation.

The experiment for sample 1 is carried out in the chamber at atmospheric pressure. The effect of alpha irradiation of sample 1 shows increasing resistance (fig. 4.15). But the same trend of increasing resistance is also shown by graphene inside the chamber without the presence of an alpha particle source. However, the change of resistance without the presence of graphene has a smaller gradient compared to the measurement with α-particles irradiation. After 5.5 hours, the sample exposed to α-particles shows the increase in the resistance reaching 139 Ω. On the other hand, the rise of the resistance of graphene inside the chamber without α-particles irradiation ends at 61 Ω.

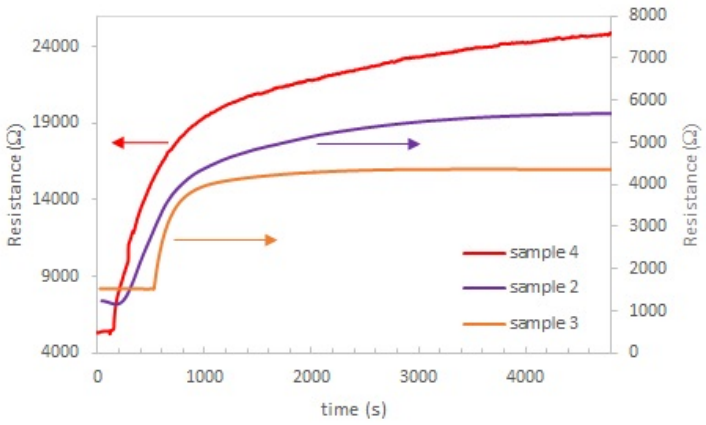

Figure 4.16: Resistance of sample 2, sample 3 and sample 4 during the pumping process.

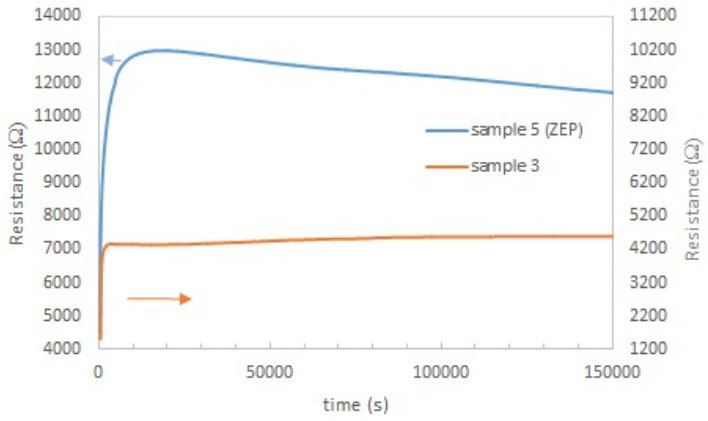

Figure 4.17: Resistance of sample 3 and sample 5 during long time pumping.

During the pumping the resistance of all samples of graphene is initially increasing very strongly. This is a result of the detachment of unintentional doping in the graphene surface during the fast reduction of the pressure that leads to a lower carrier concentration (fig. 4.16). The change of the resistance slows down after about one hour, but the time for reaching saturation condition depends on the sample as illustrated for sample 3 and sample 5 in fig. 4.17 The sample that is only supported by PMMA shows a longer time to reach saturation compared to a sample that is supported by ZEP/PMMA. After pumping to a turbo vacuum, the resistance of sample 3 starts decreasing after two days while the resistance of sample 5 decreases already after 4 hours.

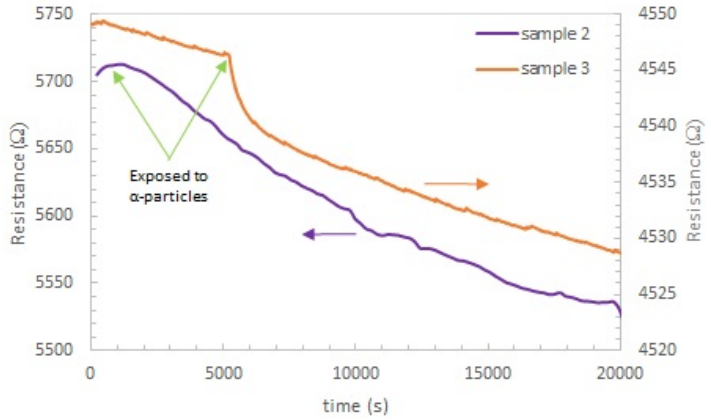

Figure 4.18: The resistance change of sample 2 and sample 3 after alpha irradiation.

At the beginning, after a graphene sample is exposed to α-particles, the resistance is always decreasing independent of their initial resistance, if it was increasing or decreasing (fig. 4.18, fig. 4.19). The first two hours of α-particles irradiation of sample 2, sample 3 and sample 4 resulted in decreasing the resistance to 97 Ω, to 12

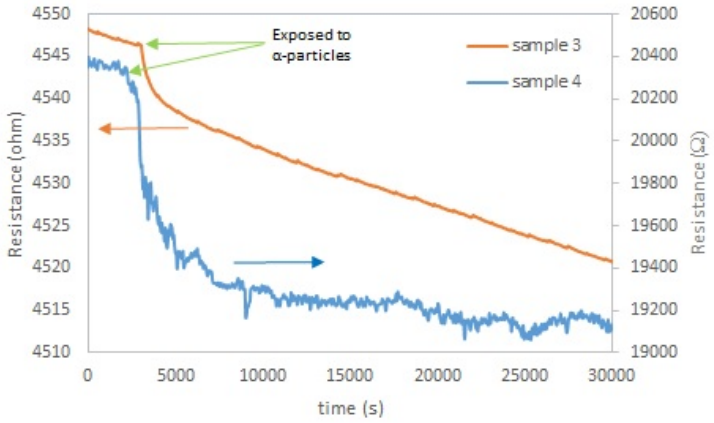

Figure 4.19: The resistance change of sample 3 and sample 4 after alpha particles irradiation. The high value of and significant of fluctation in the resistance of sample 4 are due to problems during the trasfering process, therefore the quality of this doping is rather poor compare to the other sample.

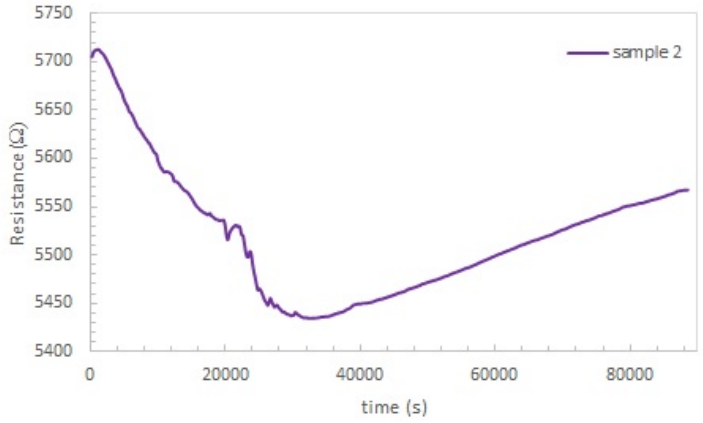

Figure 4.20: The peculiar resistance change of sample 2 under α-particles irradiation.

Ω, and to 1040 Ω respectively. The decrease of the resistance possible three possible underlying mechanisms. First, after reaching a maximum value of resistance during pumping, graphene tends to have a decreasing resistance. The decreasing resistance that continues for several days, occurres because of a rebinding of unintended doping on graphene layer that loose its interaction during previous pumping. Second, might be caused by the doping from substrate particle. The interaction of alpha particles and the substrate could result in the removal of substrate particles deposited on the graphene surface. The PMMA that behaves as p-type doping to a graphene layer affects the resistance of graphene if this process occurs. For these samples, the substrate acts as irreversible doping with the change of pressure. The doping by substrate occurs on the backside of graphene which is protected from environment

influences. The third possible mechanism is the generation of current in graphene layer. The penetration of alpha particle through the graphene layer could generate electron and hole pairs that are attracted to different direction by the potential difference created by the ohmmeter. This flow of electrons and holes is detected by the ohmmeter as decreasing of the graphene resistance.

Sample 2 (fig. 4.20) is exposed to alpha radiation before the resistance starts declining. After six hours it shows a distinctive difference compared to other samples, namely increasing resistance under alpha irradiation. This is due to the fact that the doping from PMMA and the current generation are already saturated, but doping removal due to pumping continues still. This shows that the doping by PMMA and current generation changes the graphene resistance in relatively short time. The continued changing of the graphene resistance, lasting for a long time, is mainly due to the unintended doping on the graphene surface.

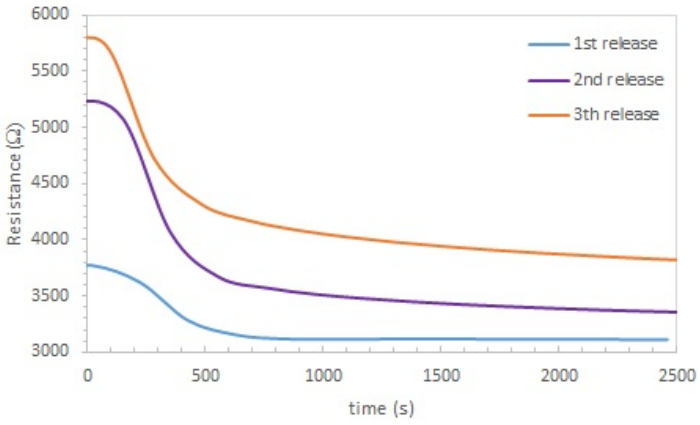

Figure 4.21: Resistance characteristic of sample 3 during three concecutive venting procedures. 1^{st} venting was carried out to the vacuum chamber after 10 minutes pumping followed by 2 hours venting. 2^{nd} venting was carried out to the vacuum chamber after 10 minutes pumping followed by 1.5 hours venting. 3^{rd} venting was carried out to the vacuum chamber after 23 hours pumping.

The venting procedures (fig. 4.21) shows that graphene needs longer time to reach its low initial resistance after each pumping phase. The physisorption occurs immediately because of the weak Van der Waals forces. Therefore, the steep part of the graphs might be caused by the physisorption process. The different level of sample 3 resistance for three conditions is due to the pumping removes the weaker chemically bonded doping. Further pumping removes more strong bonded doping. The long phase of resistance change is the slow decrease part with a higher decrease rate for the further pumping step. This indicates the doping process by chemical reaction occurs.

For graphene/PMMA samples, irreversible doping is insignificant compared to the reversible doping. During the first pumping, the graphene is exposed to alpha

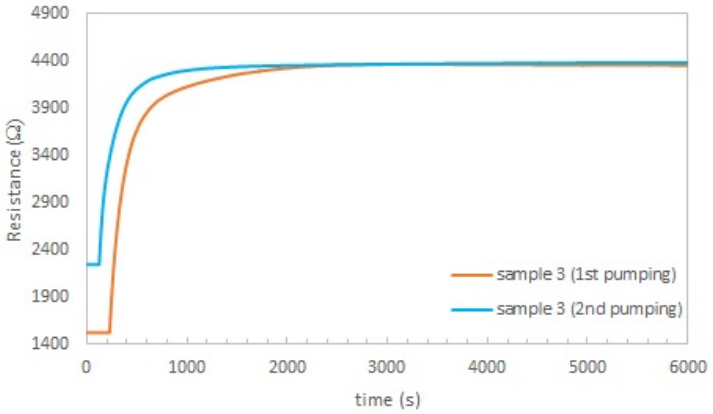

Figure 4.22: Resistance characteristic of two pumping and venting cycles for sample 3.

irradiation that is expected to result in more PMMA doping. However, the repeated venting and pumping shows that additional PMMA doping is not significant because in the second pumping graphene could reach the maximum resistance of the first sample. The second pumping stage of sample 3 (fig. 4.22) shows that graphene reach its initial resistance of the first pumping step. The faster time needed by the graphene to reach saturation in second pumping stage indicates weaker chemical bonding between gases and graphene. For the second pumping step, graphene has not been as exposed to air as before the first pumping of the sample, that is stored longer in ambient condition before the experiment is started.

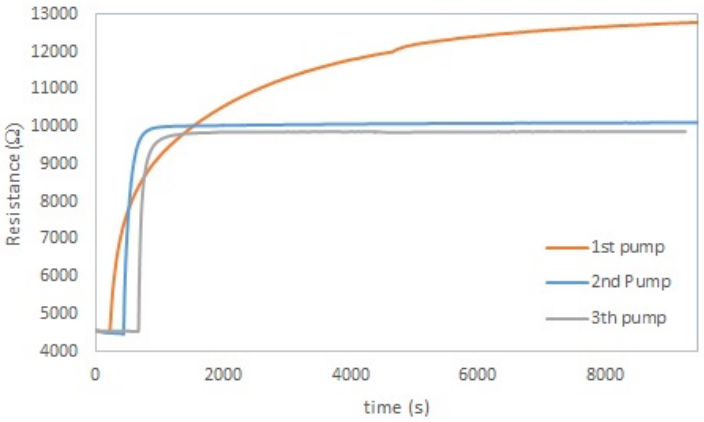

Figure 4.23: The change of resistance due to several pumping steps of sample 5. During the first and third pumping, the sample is exposed to alpha irradiation after the resistances reach saturation. During the second pumping, the source is removed.

The big difference in the saturated resistance between first and second pumping stage of the samples indicates the irreversible caused by ZEP is significant (fig. 4.23). On the other hand, the slight difference between the saturated resistance

of second and third pumping cycle sample shows that without alpha particle irradiation, irreversible doping is much smaller. The origin of the slight difference between the saturated resistance in the second and the third pumping stage is doping by chemically bonded gases as found in the graphene/PMMA sample. The rate of attachment and removal of chemically bonded gases and molecules that provide doping should be the same at graphene/PMMA and graphene/ZEP/PMMA sample because one side of graphene can interact with ambient environment freely. This indicates that the doping from ZEP is more dominant compared to the doping from PMMA.

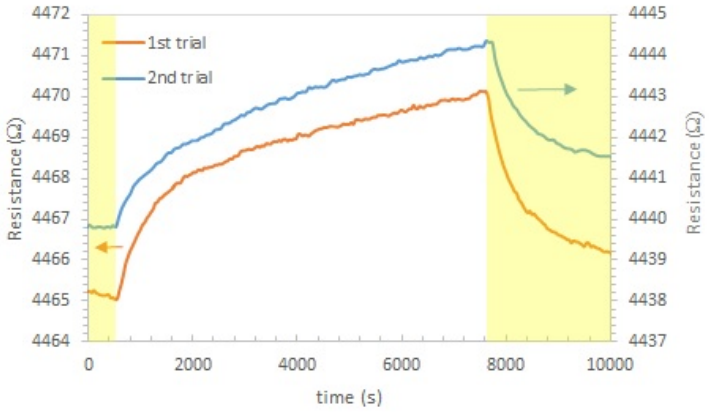

Figure 4.24: Resistance of sample 3 after interruption of α-particles exposure for two hours. The yellow region means the graphene is under alpha irradiation, while the white region means the graphene is not exposed by the alpha radiation.

Fig. 4.24 shows that the graphene resistance is increasing when alpha particle exposure is interrupted by closing of the shutter for two hours. The first trial and second trial show that the resistance of graphene decreases by 5 Ω and 5 Ω, respectively. For extracting only effect of alpha irradiation to the decrease of the resistance should be subtracted from the change of resistance due to the pumping process. The resistance of graphene before the first trial is decreasing 1 Ω/hour, while for the second trial, the change is insignificant. These numbers are obtained from the value of resistance as function of time with steady gradient before the shutter close. The effect of the stopping alpha irradiation for first and second trial increase the resistance of graphene 6 Ω and 4 Ω respectively.

If the source is removed from the set-up, the change of resistance during the closing/opening shutter does not completely disappear for sample 3 (fig. 4.25). The movement of the shutter triggers the change of resistance in a similar fashion as during irradiation. However, the magnitude of the increase of the resistance after closing the shutter is smaller. After two hours of closing the shutter, the resistance of the graphene changes only by 2 Ω. Due to pumping, the change of the resistance before closing the shutter is not significant. Therefore, the change without the source

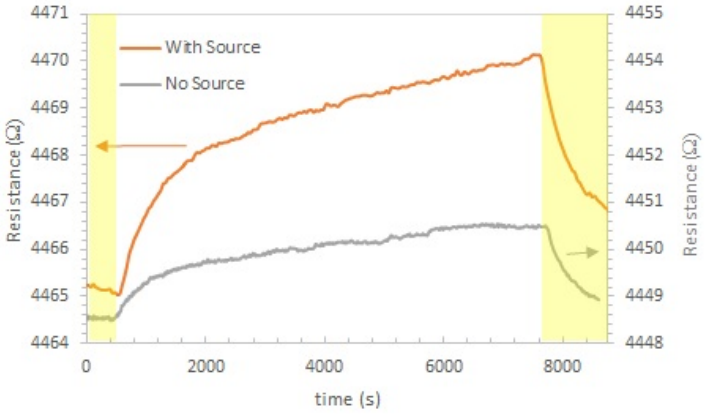

Figure 4.25: Resistance of sample 3 after interruption of α-particles exposure for two hours (orange line) and the influence of the shutter movement on the resistance of graphene (grey line). The yellow (white) region means the shutter is opened (closed).

is about half of the resistance change with the alpha irradiation.

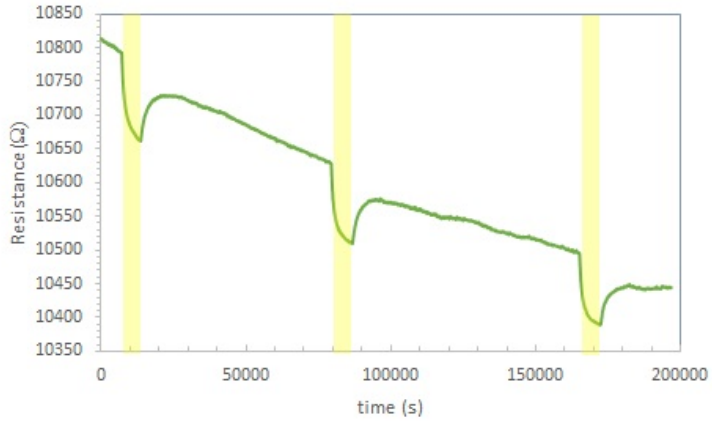

Figure 4.26: The resistance of sample 5 under alpha irradiation for two hours. The yellow means the graphene is under alpha irradiation, while the white region means the graphene is not exposed by the alpha radiation.

The resistance of the graphene sample 5 with a ZEP supporting film during two hours exposure is shown in the figure 4.26. The dips show that the resistance of graphene decreases by 120 Ω, 115 Ω, 104 Ω for the first, second and third alpha irradiation, respectively. Before the exposure, the graphene resistance has a relatively stable rate of 12 Ω/hour, 7 Ω/hour and 4 Ω/hour before the first, second and third exposure, respectively. Assuming that the rates are stable during the exposure, the net change of the resistance due to alpha irradiation is 96 Ω, 101 Ω and 96 Ω. The comparable values of the three measurements shows that the effect is rather consistent. The effect of the exposure α-particle that decrease the resistance of graphene

samples under vacuum condition is altering significantly for different samples (Table 4.6). This might be caused by the difficulties of made exactly identical graphene samples due to the significant influence of unintentional doping from environment.

Sample	Decrease of Resistance	
	Ω	%
Sample 2	97	1.7
Sample 3	12	0.3
Sample 4	1040	5.1
Sample 5	96	0.9

Table 4.6: The decrease of resistance for all samples after two hours alpha irradiation in vacuum. The percentage is calculated from the initial resistance of each sample before the alpha exposure.

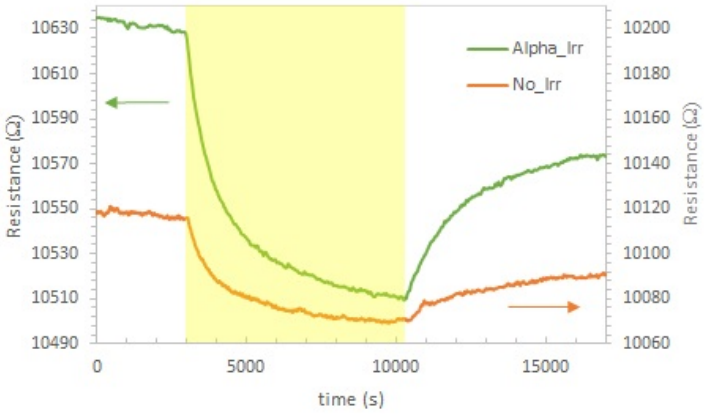

Figure 4.27: The decrease of the resistance of sample 5 due to alpha particle irradiation (green line) and shutter movement (orange line). The yellow (white) region means the shutter is opened (closed).

For comparing the effect of alpha irradiation and the shutter movement, some measurements were carried out. If the first method is used, decrease of the resistance of 116 Ω is measured. If the source is removed, the resistance decrease by 37 Ω (fig. 4.27). A similar is found using the second method. The graphene resistance increases 42 Ω after the alpha irradiation stops for two hours. If the source is removed, the graphene resistance increases 20 Ω after the shutter was closed for two hours (fig. 4.28). This result is consistent with result found with sample 3.

The aging factor of graphene is not the origin of the weaker resistance change without the alpha particle source. Fig. 4.29 and fig. 4.30 show the change of the resistance of sample 5 with and without the source by opening the shutter. The

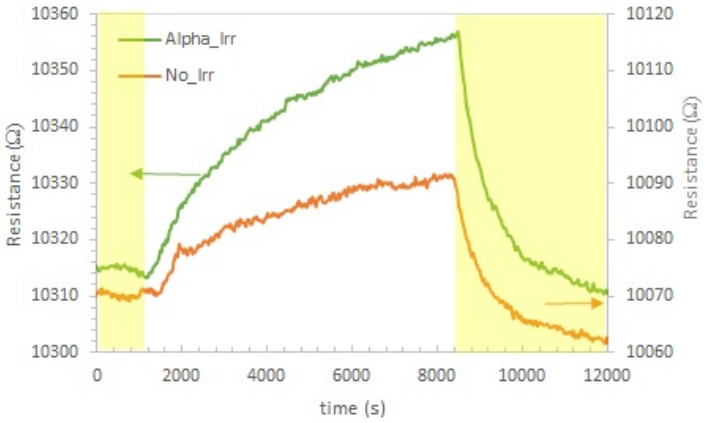

Figure 4.28: The increase of the resistance of sample 5 due to α-particle irradiation (green line) and shutter movement (orange). The yellow (white) region means the shutter is opened (closed).

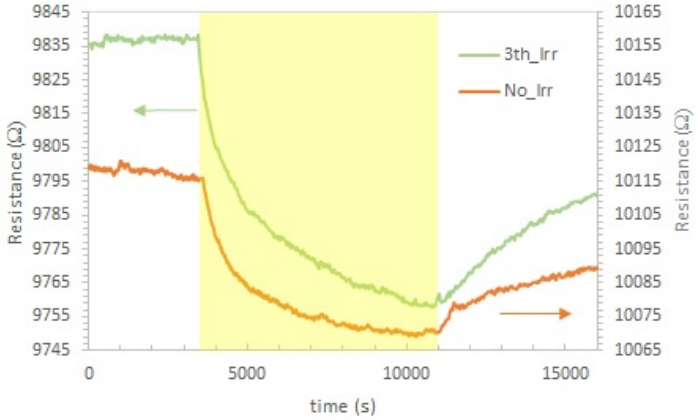

Figure 4.29: The decrease of the resistance of sample 5 (third pumping cycle) due to alpha particle irradiation (green line) and shutter movement (orange line). The yellow (white) region means the shutter is opened (closed).

measurement with no source is carried out during the second pumping cycle and the resistance change with source is measured during the third pumping stage. This demonstrates that the graphene, exposed to α-particles, has a larger decrease of resistance than graphene with no source. The decrease of the resistance under alpha irradiation and without alpha irradiation is 79 Ω and 37 Ω, respectively. If the second method is applied, the change of resistance with and without the presence of alpha particle source are 40 Ω and 20 Ω, respectively. By these facts, the exposure of alpha irradiation is the source of a significant change of graphene resistance that can be distinguishable from the influence of shutter movement.

Most of the measurement is carried out when the pressure in vacuum chamber in order of few μtorr. Observation of pressure change due to the movement of shutter

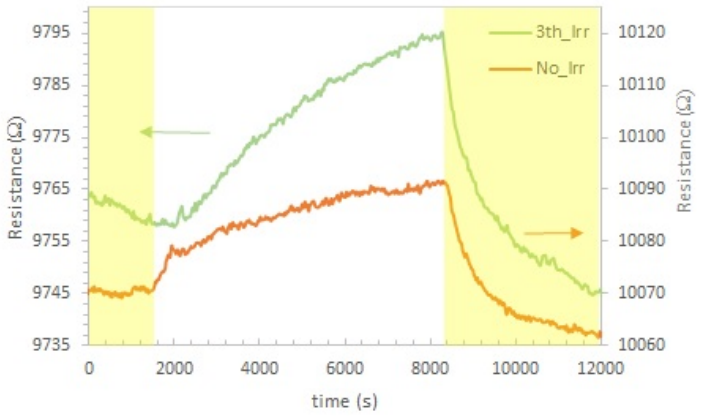

Figure 4.30: The increase of sample 5 resistance (third pumping cycle) due to the effect of an interrupting of α-particle irradiations (green line) and shutter movement (orange line). The yellow (white) region means the shutter is opened (closed).

is conducted when the pressure of vacuum chamber is stable at 1.5 μtorr. The opening of the shutter generally does not affect the pressure that is measured by a pressure gauge. The closing movement of the shutter results in a more significant pressure change. When the shutter is closed, the pressure changes to 1.8 μtorr for 30 s. Afterward, it decreased to 1.6 μtorr for 2 minutes and finally returned to its stable condition at 1.5 μtorr. Once the setup was modified so that the shutter needed to travel only a third of its length, the stability of the shutter operation was improved. The pressure change from 1.5 μtorr to 1.7 μtorr for 30 seconds before stable again at 1.5 μtorr. Several minutes after closing and opening the pressure sometimes fluctuated until reach 2.0 μtorr in about 10 seconds before the pressure returns to its stable value of 1.5 μtorr. However, based on the observation, this abrupt fluctuation does not affect the trend of the resistance change. However, the positions between the pressure gauge and the sample that are separated about 30 cm result in a possibility that the local pressure change that might be larger cannot be measured.

4.3 Signal and Current Measurement in Graphene

4.3.1 Search for Graphene Signals

For every search of graphene signals, the signals were observed by an oscilloscope that can measure magnitude and frequency of the signals. Before the signal were observed by oscilloscope, those signals had been proceeded by some amplification steps. The signal was tried to observed; the first after Preamplifier, the second after Preamplifier and Spectroscopy Amplifier, the third after Preamplifier and Timing Filter Amplifier. During the searching, shaping time constant was also altered to

find the optimum range of frequencies that might be effective to separate signals from noises.

Sample 2, sample 3 and sample 5 were biased through the preamplifier with potential from a few tens of volts up to 600 V. With the information about the voltage devider circuit inside the preamplifier, we could estimate the voltage bias between two contacts of the graphene layer to be about 30 mV when 600 V preamplifier bias was given. With that arrangement the current that passed through the graphene layer is about 28 μA. However, using these setup no signal could be detected. Next trial, the sample 3 was biased with a higher voltage by connecting it to 9 V battery with a voltage divider circuit and a potentiometer. The voltage bias of graphene is set to be about 1.3 V and 9.4 V. With this configuration, the oscilloscope also detected no signal from the graphene sample.

A possible reason for the absence of the signal is that the current produced by alpha irradiation in graphene layer is too small. The order of the current that could be below a femto ampere makes distinguishing the signal from electronic noise became difficult. For the reference, the typical induced peak current from a semiconductor detector is about 1 μA for 10^5 radiation-induced charges [45]. The reason for the weak current signals might be either the excitation of carrier during the alpha irradiation was not sufficient or there were plenty of carrier excitations but the electric field needed to attract the carriers was weak.

4.3.2 Current Measurement

The generation of current might be a reason for the change of the graphene resistance. All measurements that involve alpha irradiation show a change of the resistance of the graphene layer after exposure. This indicates that irradiation causes a reversible process. The reason for this could be that alpha irradiation disturbs interactions between the doping and the graphene layer or that alpha particles generate a current in the graphene layer. current measurements were carried out by applying different voltage bias to graphene contacts (fig. 4.31). The measurement were conducted under two conditions, with and without alpha irradiation. As discussed before, irradiation alters the resistance for some hours before saturated. Therefore, the measurements were carried out after the resistance of sample 5 reached a stable value.

The effect of alpha irradiation was studied by measuring the current difference versus the voltage bias for both conditions (fig. 4.32). The results indicate that there is always current difference present for both conditions. This result shows the additional current that affected by alpha irradiation has a value of less than 1 μA under low voltage bias. That the increase of the current difference is proportional to the voltage bias demonstrates that the current generated by the alpha particles in the sample is more significant at higher voltages.

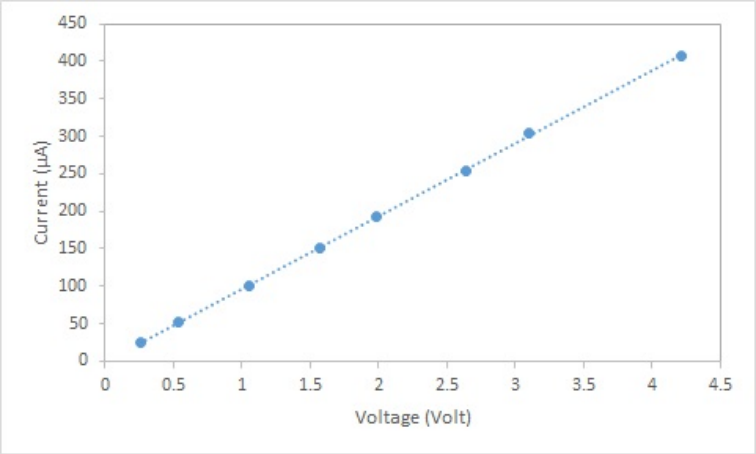

Figure 4.31: Current vs voltage bias change of the sample 5.

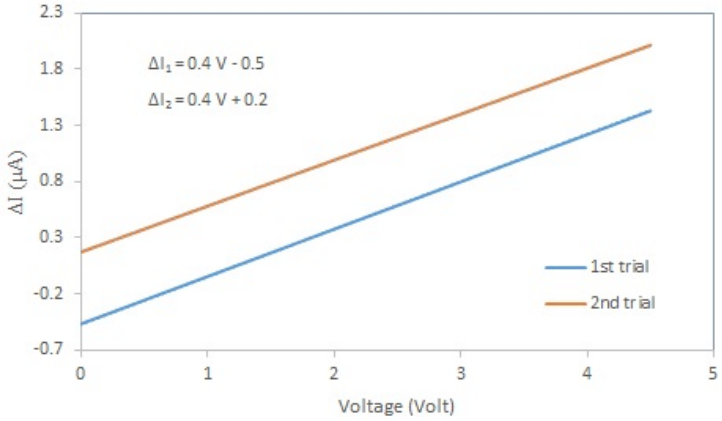

Figure 4.32: Change of current vs voltage bias change for sample 5 graphene with and without alpha irradiation.

4.4 Difficulties

The mechanisms of e-h generation and recombination in graphene are similar to those of semiconductors. Theoretically, using graphene as particle detector should work similar to a standard semiconductor detector. However, an effective separation method for electrons and holes in graphene is an important point, because the recombination time in graphene is shorter than semiconductor. Furthermore, a semiconductor detector, that is significantly thicker than a one-atom-thick of graphene layer, results in more e-h pairs from a longer ion trace. In this respect, graphene has a lower probability to create a signal that can be detected.

Beside its exceptional properties, graphene also has some weaknesses. Although it has a very high Young modulus, graphene is relatively brittle compared to metals. This is shown by the small number crack resistance. Graphene has fracture toughness in the same order as ceramic [55, 56]. Therefore, cracks in graphene layer build

up and propagate easily during the fabrication, transfer and measurement. Besides, the energy state of graphene is easily perturbed by adatom functionalization from growth process and transfer process [57] as well as during storing [58].

In this experiment, the Raman characterization could not be conducted. The challenge to use Raman spectroscopy in a graphene-PMMA sample is the transparent layer transmits most of the electromagnetic radiation and only a small part of the energy is absorbed by the sample. The other problem is that the surface of graphene is not sufficiently flat to measure the Raman spectrum. Those two problems Raman spectra, normally effective for measuring the defects in graphene, cannot be obtained [59]. Furthermore, the defining the position of the Raman spectrum should be very precise for a sample. The observed point before and after the measurement should be precisely the same. Otherwise, the resulting spectrum is not reliable for detecting graphene defects caused by measurements.

The current that results from a resistance measurement depends on the measured resistance. The ohmmeter generates a smaller current for a larger resistance (Table 3.1). The difference in currents might create a different graphene responses. A larger current could evaporate water molecules on the top of a graphene sample faster. The non-uniformity of the current can affect the consistency of resistance change under alpha irradiation for different samples with difference range of resistance.

No.	Measurement Range	Test Current
1	100 Ω	1 mA
2	1 kΩ	1 mA
3	10 kΩ	100 μA
4	100 kΩ	10 μA
5	1 MΩ	1 μA
6	10 MΩ	0.1 μA
7	100 MΩ	0.1 μA

Table 4.7: The magnitude of test currents of the Ohmmeter during resistance measurements [60]

5

Conclusion

5.1 Conclusion

Graphene is very sensitive to ambient conditions. Therefore, the direct effect of alpha particle irradiation is often hard to distinguished from the effect of external parameters. Besides, the initial conditions and electronic behavior of all graphene samples are varied for all measurements. Due to the fact that the reproducibility of a measurement with exactly the same conditions is not an easy task to accomplish.

The single layer of graphene acquires negligible part of alpha particle energy during irradiation. Most part of the energy loss is deposited in the PMMA and ZEP substrates. This make it hard to detect any electronic signal from the a single layer graphene detector.

Based on the results of the experiments, the possibilities to makes a particle detector based graphene are not yet clear. Nonetheless graphene shows high permeability, high durability, and capability to result in small current under alpha particles irradiation gives hopes that graphene could be designed as a future particle detector.

5.2 Outlook

The fabrication of vertical structure P-N junction graphene is worth to try for separating electron-hole pairs efficiently, while preventing the inherently high recombination rate of pristine graphene. With this vertical sturcture, the characterization of graphene can be carried out by a standard field effect characterization method. The structure behaves as a field effect device, so the back-gate voltage is readily generateded to obtain information about the quality and change of properties for both sides of the graphene layer by merely measuring its source-drain current. The standard field effect characterization also capable of revealing some fundamental properties of graphene sample such as the type and the level of doping. On the other hand, by applying perpendicular electric field to a graphene layer, more carriers could be produces for increasing the sensitivity because the interaction of the particles with the carriers has a higher probability for higher carrier concentration.

For future experiments on the use of graphene as ion detector, multilayers of graphene might be interesting because more energy from the alpha particles is deposited. On the other hand, searching for other supporting films that could produce

more electrons scattering during the irradiation is also key for generating electronic signals from graphene layer.

Due to the ultrasensitive behavior of graphene electronic properties upon reaction with environment particles, the graphene sample should be passivated. This could be carried out with deposition of encapsulated thin film of graphene to prevent direct contact of graphene with the environment. This is known to prevent unintentional functionalization on the graphene surface and edges resulting in a higher stability of graphene device [58].

References

[1] Chang-Hua Liu *et al.* Graphene photodetectors with ultra-broadband and high responsivity at room temperature, Nature Nanotechnology, 9, 273–278 (2014)

[2] Xuetao Gan *et al.* Chip-integrated ultrafast graphene photodetector with high responsivity, Nature Photonics, 7, 883–887 (2013)

[3] F. H. L. Koppens *et al.* Photodetectors based on graphene, other two-dimensional materials and hybrid system. Nature Nanotechnology, 9, 780–793 (2014)

[4] G. H. Lu, L. E. Ocola and J. H. Chen. Reduced graphene oxide for room-temperature gas sensors, Nanotechnology, 2009, 20, 445502.

[5] H. Y. Jeong, D. S. Lee, H. K. Choi, D. H. Lee, J. E. Kim, J. Y. Lee, W. J. Lee, S. O. Kim and S. Y. Choi,Flexible room-temperature NO2 gas sensors based on carbon nanotubes/reduced graphene hybrid films, Appl. Phys. Lett., 2010, 96, 3432446.

[6] V. Dua, S. P. Surwade, S. Ammu, S. R. Agnihotra, S. Jain, K. E. Roberts, S. Park, R. S. Ruoff and S. K. Manohar, All-Organic Vapor Sensor Using Inkjet-Printed Reduced Graphene Oxide, Angew. Chem., Int. Ed., 2010, 49, 2154–2157.

[7] J. D. Fowler, M. J. Allen, V. C. Tung, Y. Yang, R. B. Kaner and B. H. Weiller, Practical Chemical Sensors from Chemically Derived Graphene, ACS Nano, 2009, 3, 301–306

[8] P. K. Ang, W. Chen, A. T. S. Wee and K. P. Loh, Solution-gated epitaxial graphene as pH sensor, J. Am. Chem. Soc., 2008, 130, 14392–14393.

[9] T. Zhang, Z. G. Cheng, Y. B. Wang, Z. J. Li, C. X. Wang, Y. B. Li and Y. Fang, Self-Assembled 1-Octadecanethiol Monolayers on Graphene for Mercury Detection, Nano Lett., 2010, 10, 4738–4741

[10] H. G. Sudibya, Q. Y. He, H. Zhang and P. Chen,Electrical Detection of Metal Ions Using Field-Effect Transistors Based on Micropatterned Reduced Graphene Oxide Films, ACS Nano, 2011, 5, 1990–1994.

[11] F. Schedin *et al.* Detection of individual gas molecules adsorbed on graphene. Nature Materials 6, 652 - 655 (2007)

[12] Jeremy T. Robinson *et al.* Reduced Graphene Oxide Molecular Sensors. Nano Lett., 2008, 8 (10), pp 3137–3140

[13] Lee, C. *et al.* Measurement of the Elastic Properties and Intrinsic Strength of Monolayer Graphene. Science 321, 385-388 (2008)

[14] Moser, J. *et al.* Current-induced cleaning of graphene. Appl. Phys. Lett. 91. 163513 (2007)

[15] Mayorov, A. S. *et al.* Micrometer-Scale Ballistic Transport in Encapsulated Graphene at Room Temperature. Nano Lett. 11, 2396-2399 (2011)

[16] Yanqing Wu *et al.* High-frequency, scaled graphene transistors on diamond-like carbon. Nature, 472, 2011

[17] Yu-Ming Lin *et al.* Operation of Graphene Transistors at Gigahertz Frequencies. Nano Letter 2009 Vol. 9, No. 1 422-426

[18] J Hopster *et al.* Damage in graphene due to electronic excitation induced by highly charged ions. 2D Mater. 1 011011 (2014)

[19] B. T. Kelly. Physics of graphite. London: Applied Science Publishers, 1981.

[20] M. Mahendran. The Modulus Elasticity of Steel - Is it 200 GPa? Thirteenth International Specialty Conference on Cold-Formed Steel Structures St. Louis, Missouri U.S.A., October 17-18,1996

[21] Chia-Liang Sun, Chun-Yi Chiu, System for manufacturing graphene nanoribbon by continuous microwave, United States patent US 20150050193 A1. Feb 19, 2015

[22] Hongtao Liu *et al.* Chemical doping of graphene. J. Mater. Chem., 2011, 21, 3335–3345

[23] Sunmin Ryu *et al.* Atmospheric Oxygen Binding and Hole Doping in Deformed Graphene on a SiO2 Substrate. Nano Lett. 2010, 10, 4944⁻4951

[24] G. Giovannetti *et al.* Doping Graphene with Metal Contacts. PRL 101, 026803 (2008)

[25] http://hyperphysics.phy-astr.gsu.edu/hbase/tables/photoelec.html

[26] Jian-Hao Chen *et al.* Printed Graphene Circuits. Adv. Mater. 2007, 19, 3623–3627

[27] O. Ochedowski *et al.* Radiation hardness of graphene and MoS2 field effect devices against swift heavy ion irradiation. Journal of Applied Physics 113, 214306 (2013)

[28] Li Li Zhang *et al.* Nitrogen doping of graphene and its effect on quantum capacitance, and a new insight on the enhanced capacitance of N-doped carbon. Energy Environ. Sci., 2012, 5, 9618–9625

[29] Sunmin Ryu *et al.* Atmospheric Oxygen Binding and Hole Doping in Deformed Graphene on a SiO2 Substrate. Nano Lett. 2010, 10, 4944–4951

[30] Jean-Marie Aubry *et al.* Reversible Binding of Oxygen to Aromatic Compounds. Acc. Chem. Res. 2003, 36, 668-675

[31] Frank schwierz. Graphene transistors. nature nanotechnology, 5, 2010

[32] Eduardo V. Castro. Biased Bilayer Graphene: Semiconductor with a Gap Tunable by the Electric Field Effect. PRL 99, 216802 (2007)

[33] L.M. Malard *et al.* Raman spectroscopy in graphene. Physics Reports 473 (2009) 51–87

[34] Zheng YanAndrew R. Barron. http://cnx.org/contents/f06226c5-c2a4-4798-9c75-b016acea73cd@2/Characterization-of-Graphene-b

[35] A. Gupta *et al*, Raman Scattering from High-Frequency Phonons in Supported n-Graphene Layer Films. Nano Letter 2006 Vol. 6, No. 12 2667-2673

[36] Some, S. *et al* (2012), Highly Air-Stable Phosphorus-Doped n-Type Graphene Field-Effect Transistors. Adv. Mater., 24: 5481–5486. doi:10.1002/adma.201202255

[37] J.H. Chen *et al.* Charged-impurity scattering in graphene. Nature Physics, vol 4, 2008

[38] Vassilios Fessatidis *et al.* Graphene energy loss spectroscopy: Perpendicular case. Physics Procedia 3 (2010) 1279–1285

[39] E. H. A. Algren. Ion irradiation tolerance of graphene as studied by atomistic simulations. Applied Physics Letters 100, 233108 (2012)

[40] G. Labaigt *et al.* Electron capture imaging of two-dimensional materials. Physical Review B 89, 245438 (2014)

[41] O. Lehtinen *et al.* Effects of ion bombardment on a two-dimensional target: Atomistic simulations of graphene irradiation. PHYSICAL REVIEW B 81, 153401 2010

[42] Sunil Kumar *et al.* Radiation stability of graphene under extreme conditions. Appl. Phys. Lett. 105, 133107 (2014)

[43] Jin-Wu Jiang. Graphene Versus MoS2: a Mini Review. arXiv:1408.0437v2 [cond-mat.mtrl-sci] 12 Feb 2015

[44] S. Hu *et al.* Proton transport through one-atom-thick crystals. Nature, Vol 516, 2014, page 227

[45] Knoll, G. F. Radiation Detection and Measurement. John Wiley and Sons (1989)

[46] Private conversation with Andreas Heinz and Thomas Nilsson.

[47] F. Rana. Electron-hole generation and recombination rates for Coulomb scattering in graphene. Physical Review B 76, 155431 2007

[48] P. Harrison, Quantum Wells, Wires and Dots Wiley, New York, 2005.

[49] Kiril Koshelev *et al.* Comparison between ZEP and PMMA resists for nanoscale electron beam lithography experimentally and by numerical modelling. J. Vac. Sci. Technol. B 29 (6), Nov/Dec 2011

[50] A. M. S. Galante *et al.* Comparative study of the dose rate influence in the radiochromic polymeric film dosimeter response. Journal of Physics: Conference Series 249 (2010) 012061

[51] G. Espinosa and R. J. Silva. Alpha-particle analysis of a triple isotope 239Pu – 241Am – 244Cm source by nuclear track methodology. Journal of Radioanalytical and Nuclear Chemistry, Vol. 248, No. 3 (2001) 575–578

[52] http://www.graphenea.com/products/monolayer-graphene-on-cu-1-inch-x-1-inch

[53] K. J. Tielrooij *et al.* Photoexcitation cascade and multiple hot-carrier generation in graphene. Nature Physics, Vol. 9, 2013

[54] http://physics.nist.gov/cgi¯bin/Star/ap_table.pl

[55] Zhang, P. *et al.* Fracture toughness of graphene. Nat. Commun. 5:3782 doi: 10.1038/ncomms4782 (2014).

[56] George A Gogotsi. Fracture toughness of ceramics and ceramic composites. Ceramics International 29 (2003) 777–784

[57] Jamie H. Warner *et al.* Sensitivity of Graphene Edge States to Surface Adatom Interactions. Nano Lett. 2013, 13, 4820¯4826

[58] Abhay A. Sagade *et al.* Highly air stable passivation of graphene based field effect devices. Nanoscale, 2015, 7, 3558

[59] Private conversation with Grigory Soblin

[60] Jerry Janesch. Two-Wire vs. Four-Wire Resistance Measurements: Which Configuration Makes Sense for Your Application? Keithley Instruments, Inc. 2013